

# Numerical Prediction of Three-Dimensional Non-Equilibrium Flows Using the Regularized Gaussian Moment Closure

C. K. S. Lam\* and C. P. T. Groth†

*University of Toronto Institute for Aerospace Studies  
4925 Dufferin Street, Toronto, Ontario, Canada, M3H 5T6*

A parallel, implicit, adaptive mesh refinement (AMR), finite-volume scheme is described for the solution of the regularized Gaussian moment closure. The latter incorporates the influences of heat transfer by means of a first-order correction to the standard Gaussian closure. The combined moment closure treatment / numerical method is applied to the prediction of three-dimensional, non-equilibrium, micro-scale, gaseous flows. Unlike other regularized moment closures, the underlying maximum-entropy Gaussian closure provides a fully-realizable and strictly hyperbolic description of non-equilibrium gaseous flows that is valid from the continuum limit, through the transition regime, and up to the near-collisionless, free-molecular flow limit. The regularized closure provides a similarly robust description than now includes a fully anisotropic description of heat transfer. The proposed finite-volume scheme makes use of Riemann-solver-based flux functions and limited linear reconstruction to provide accurate and monotonic solutions, even in the presence of large solution gradients and/or under-resolved solution content on three-dimensional, multi-block, body-fitted, hexahedral mesh. A rather effective and highly scalable parallel implicit time-marching scheme based on a Jacobian-free inexact Newton-Krylov-Schwarz (NKS) approach with additive Schwarz preconditioning and domain partitioning following from the multi-block AMR mesh is used to obtain solutions to the non-linear ordinary-differential equations that result from finite-volume spatial discretization procedure. Details are given of the regularized Gaussian closure, with suitable extensions for diatomic gases, and slip-flow boundary treatment. Numerical results for several canonical flow problems demonstrate the potential of the regularized closures, that when combined with an efficient parallel solution method, provide an effective means for accurately predicting a range of fully three-dimensional non-equilibrium gaseous flow behavior.

## I. Introduction

### A. Transition-Regime Micro-Scale Flows

Generalized fluid dynamic behavior is commonly described through the Navier-Stokes equations. This near-equilibrium transport model has proven itself to be accurate when modeling many problems typically encountered in the aerospace industry. However, the underlying assumption that the fluid behaves as a continuum breaks down when the mean free path for collisions between the fluid molecules is comparable in size to the characteristic length of the problem. At the other end of the spectrum, the modeling of rarefied flows is governed by the Boltzmann equation, and, in this regime, is more readily solved using a variety of particle simulation techniques.<sup>1</sup> The advent of micro-scale technologies<sup>2</sup> and upper atmospheric aerospace research<sup>3</sup> has prompted a need to model fluid flow behavior lying between these two regimes, where non-equilibrium effects are significant but particle simulation techniques become prohibitively costly. Proper modeling of this transition regime is critical for understanding the behavior of various macroscopic properties used in the overall design and function of these technologies.

\*Ph. D. Candidate, Email: lam@utias.utoronto.ca

†Professor, Email: groth@utias.utoronto.ca, Senior Member AIAA

## B. Moment Closures

Evaluation of non-continuum fluid flow behavior is commonly based on a statistical description of fluid particle movement, either through numerical approaches, such as a direct discretization of the Boltzmann equation and particle simulation methods,<sup>1</sup> or through approximate techniques for the Boltzmann equation.<sup>4,5</sup> Approximate techniques based on kinetic theory eventually lead to sets of coupled non-linear partial differential equations that describe the transport of macroscopic quantities. The classical mechanics concerning particle collisions are fully incorporated into these descriptions and the evolution of the particle distribution functions can be obtained. The resulting formulations can be used to derive the governing equations used in continuum flow, and can also provide the key to describing fluid flow behavior in the non-equilibrium transition regime.

The use of moment methods for non-equilibrium gases was first hypothesized by Maxwell.<sup>6</sup> Later, Boltzmann provided a means with which to study the evolution of these distribution functions, which in turn gave transport equations for various macroscopic properties.<sup>7</sup> However, the construction of the resulting moment equations is such that each transport equation relies on the flux of a higher-order velocity moment *ad infinitum*. One approach to closing off this set of equations for practical purposes is to assume a particular form for the non-equilibrium distribution function having a fixed number of free parameters in such a way that the higher-order closing velocity moment can be expressed solely in terms of lower ones. Grad<sup>4</sup> considered moment closures based on a truncated polynomial power series expansion for the approximate distribution function and this technique generated first-order systems of hyperbolic partial differential equations (PDEs) describing the time evolution of the macroscopic moments. However, hyperbolicity of the Grad moment equations is not guaranteed for all flow conditions leading to closure breakdown and the assumed form for the distribution function is not always physically plausible.

An alternative hierarchy of maximum-entropy moment closures has been developed by Levermore.<sup>5</sup> The Levermore hierarchy has a number of desirable mathematical properties including strict hyperbolicity, thus the possibility of closure breakdown in this sense is avoided. The lowest order of this hierarchy of closures is the 5-moment closure that corresponds to the Euler equations, while the next member results in the 10-moment closure, also known as the Gaussian closure. While a full guarantee of both moment realizability and hyperbolicity applies only to these two lowest-order closures in the hierarchy,<sup>8</sup> the usefulness of such closures is evident from a computational standpoint. Being purely hyperbolic with only first-order derivatives, the solution is guaranteed to have finite speeds of propagation. Moreover, numerical solutions can be readily obtained using the highly successful class of Godunov-type finite volume schemes developed for hyperbolic conservation laws without excessive modification.<sup>9</sup> These schemes are robust, accurate, and can preserve the conservation properties of the solution at the discrete level. They can also be applied using a large variety of boundary conditions and meshing techniques and, for first-order systems, provide solutions that are generally rather insensitive to irregularities in the mesh.

While the Gaussian closure is a somewhat simplified mathematical model, as it does not incorporate the effects of heat transfer, it has been shown to accurately describe non-equilibrium momentum transport for a range of micro-scale flows and is very representative of other higher-order closures that would potentially include the effects of non-equilibrium thermal transport.<sup>10-12</sup> The numerical solution and application of the Gaussian closure for two-dimensional micro-scale flows has been studied extensively by McDonald and Groth,<sup>10-12</sup> with considerations for diatomic gases following the approach devised by Hittinger<sup>13</sup> as well as with a regularization correction for heat transfer effects.<sup>11</sup> A discontinuous Galerkin finite-element solution scheme for the Gaussian closure has also been proposed by Barth<sup>14</sup> and additional research by Levermore *et al.*<sup>15</sup> has been performed on one-dimensional shock structures taken from the Gaussian closure. These studies have shown the computational robustness of the Gaussian closure over a wide range of Knudsen numbers and has encouraged the development of the fully three-dimensional solution procedure outlined here for both academic and industrial purposes.

The lack of heat transfer in the Gaussian closure becomes an issue that cannot be ignored given its otherwise attractive computational properties. Work by Struchtrup and Torrilhon<sup>16-19</sup> has explored the regularization of the Grad moment closure for describing higher order effects through a Chapman-Enskog-type perturbative expansion about the moment equations to allow for small deviations from the assumed form of the distribution function. The regularized forms of the Grad 13-moment and 26-moment closures have been shown to be accurate in the prediction of non-equilibrium phenomena such as velocity and temperature slip at solid boundaries, and the accurate modeling of one-dimensional shock structures that deviate significantly from thermodynamical equilibrium. While promising, the underlying hyperbolic moment system can still suffer from the those of the original Grad moment closure mentioned above, namely the loss of hyperbolicity

even for small deviations from equilibrium.

McDonald and Groth<sup>11,20</sup> have recently applied a similar regularization procedure on the Gaussian closure for two-dimensional, heat-conducting flow directly based on the anisotropic pressure tensor. While the regularization process adds an additional elliptic term to the otherwise hyperbolic set of equations, the underlying first-order moment system remains hyperbolic for the full range of physically realizable moments. The computational advantages and modeling potential for this approach to non-equilibrium flows has now prompted its advancement for the modeling of fully three-dimensional flows.

### C. Scope of Study

The main objective of this work is to consider the efficient numerical solution and subsequent application of the regularized Gaussian moment closures that incorporates the effects of heat transfer, functionality that is inherently missing in the Gaussian closure. The regularized closure is applied to the modeling of three-dimensional non-equilibrium micro-scale flows with the aid of a new parallel implicit adaptive mesh refinement (AMR) finite volume scheme for solving the moment equations on multiblock, body-fitted hexahedral mesh. The proposed AMR allows for a local refinement of the computational mesh based on a procedure by Gao and Groth.<sup>21–23</sup> The solution procedure developed for solving the generalized transport equations of the regularized Gaussian-based closures is accelerated with a parallel Newton-Krylov method with additive Schwarz preconditioning. Verification and assessment of the capabilities of the approach has been conducted by considering its application to a number of canonical three-dimensional steady state flow problems.

## II. Regularized Gaussian Closures

### A. Gaskinetic Theory

The kinetic theory of gases begins by treating the gas as a collection of discrete microscopic particles that interact with each other and the walls of its container through collisional processes to create perceived macroscopic properties such as density and pressure. Energy transfer between particles and its container are solely described by classical mechanics subject to Newton's laws of motion. However, constructing a set of equations describing the motion of individual particles becomes computationally prohibitive for all but the most rarefied of flow conditions.

Treatment of the particles in kinetic theory is done instead through a statistical description, and the evolution of this probability density function is correlated directly to the macroscopic properties of the fluid medium. As particle position and velocity are independent of each other, a complete statistical description can be given by a six-dimensional phase space distribution spanning three-dimensional physical space,  $x_i$ , and velocity space,  $v_i$ , at a particular moment in time,  $t$ . The resulting probability density function,  $\mathcal{F}(t, x_i, v_i)$ , describes the number of particles occupying an elemental volume in the six-dimensional physical-velocity space at a particular moment in time.

The time evolution of  $\mathcal{F}$  is governed by the Boltzmann equation,<sup>24–26</sup> an integro-differential equation having the form

$$\frac{\partial \mathcal{F}}{\partial t} + v_i \frac{\partial \mathcal{F}}{\partial x_i} + a_i \frac{\partial \mathcal{F}}{\partial v_i} = \frac{\delta \mathcal{F}}{\delta t}, \quad (1)$$

where  $a_i$  is the acceleration due to external forces and is taken to be zero in the present work. The term on the right-hand side of the equation,  $\delta \mathcal{F} / \delta t$ , is the Boltzmann collision operator representing the time rate of change of the distribution function produced by binary inter-particle collisions. This term involves a multi-dimensional integral over both velocity space and solid angle.

Macroscopic properties of the gas can be obtained by taking appropriate velocity moments of  $\mathcal{F}$ . This is done by multiplying the distribution function by a velocity-dependent weight,  $M(v_i)$ , and integrating over all velocity space as follows:

$$\langle M(v_i) \mathcal{F} \rangle = \int_{-\infty}^{\infty} M(v_i) \mathcal{F}(t, x_i, v_i) d^3 v. \quad (2)$$

If the gas particle mass,  $m$ , is chosen as the weight (i.e.,  $M(v_i) = m$ ), the corresponding velocity moment

yields the fluid density given by

$$\rho(t, x_i) = \int_{-\infty}^{\infty} m\mathcal{F}(t, x_i, v_i) d^3v = \langle m\mathcal{F} \rangle. \quad (3)$$

Other moments of interest include the bulk velocity ( $M(v_i) = mv_i$ ),

$$u_i(t, x_\alpha) = \frac{\langle mv_i\mathcal{F} \rangle}{\rho}, \quad (4)$$

and second-order anisotropic pressure tensor ( $M(v_\alpha) = mc_i c_j$ ),

$$P_{ij}(t, x_\alpha) = \langle mc_i c_j \mathcal{F} \rangle, \quad (5)$$

where here  $c_i = v_i - u_i$  is the random component of particle velocity. The deviatoric or fluid stress tensor,  $\tau_{ij}$ , is related to the pressure tensor as  $\tau_{ij} = \delta_{ij}p - P_{ij}$ , where  $p$  is the thermodynamic pressure. Using the ideal gas equation of state, the pressure,  $p$ , is given by

$$p = \rho RT, \quad (6)$$

where  $T$  is the gas temperature and  $R$  is the gas constant. For a monatomic gas,  $\tau_{ij}$  is traceless (i.e.,  $\tau_{kk} = 0$ ) such that  $P_{kk} = 3p$  and  $T$  is a measure of the energy of the random translational motion of the gaseous particles. However, for non-equilibrium diatomic and polyatomic gases, this relationship does not generally hold and  $\tau_{kk} \neq 0$  and  $P_{kk} \neq 3p$ . For the latter,  $P_{kk} = 3p - \tau_{kk}$  and  $T$  will be taken to be the temperature of the translational modes, which are not necessarily in equilibrium with the other internal energy modes of the particle (i.e., rotational and vibrational modes).

Under conditions of thermodynamic equilibrium, the solution to the Boltzmann equation for a monatomic gas is  $\mathcal{F} = \mathcal{M}$  where  $\mathcal{M}$  is the well-known Maxwell-Boltzmann or Maxwellian distribution function given by

$$\mathcal{F}(t, x_i, c_i) = \mathcal{M}(t, x_i, c_i) = \frac{(\rho/m)}{(2\pi)^{3/2} (p/\rho)^{3/2}} \exp\left(-\frac{1}{2} \frac{\rho}{p} c^2\right), \quad (7)$$

which is fully defined in terms of the conserved macroscopic moments or collisional invariants  $\rho, \rho u_i$ , and  $p$ . The Maxwellian distribution function,  $\mathcal{M}$ , fully defines the equilibrium behavior of the gas. It can be shown that the collision operator,  $\delta\mathcal{F}/\delta t$ , will force all non-equilibrium solutions of the distribution function towards this equilibrium solution, and, once in this state, the collision operator will produce no further net changes to the distribution function. This entropy property of the collision operator is well established by Boltzmann's H theorem.<sup>26</sup>

## B. Moment Equations

Transport equations governing the time evolution of general sets of macroscopic quantities can be derived by evaluating velocity moments of the Boltzmann equation given above, Eq. (1). This yields the so-called Maxwell's equation of change<sup>26</sup> describing the transport of the moment  $\langle M(v_\alpha)\mathcal{F} \rangle$ , which can be expressed in weak conservation form as

$$\frac{\partial}{\partial t} \langle M(v_\alpha)\mathcal{F} \rangle + \frac{\partial}{\partial x_i} \langle v_i M(v_\alpha)\mathcal{F} \rangle = \Delta(\langle M(v_\alpha)\mathcal{F} \rangle), \quad (8)$$

where here the acceleration is now taken to be zero,  $\Delta(\langle M(v_\alpha)\mathcal{F} \rangle) = \langle M(v_\alpha)(\delta\mathcal{F}/\delta t) \rangle$  represents the effect of collisions on the moment quantity, and  $M(v_\alpha)$  is the appropriate velocity dependent weight.

It is at this point that the problem of closure becomes apparent for moment method techniques. The time evolution of a moment  $\langle M(v_\alpha)\mathcal{F} \rangle$  is clearly dependent on the spatial divergence of  $\langle v_i M(v_\alpha)\mathcal{F} \rangle$ , a moment of one order higher in terms of the velocity,  $v_i$ . This pattern is repeated for each moment with the time evolution of every moment being dependent on a moment of one higher order in  $v_i$ . In general, the application of the method of moments to a general non-equilibrium gas in this straightforward manner would therefore require the solution of an infinite number of coupled moment equations, the solution of which is equivalent to solving Eq. (1), which is obviously not practical.

### C. BGK Collision Operator

As mentioned previously, the evaluation of the Boltzmann collision operator involves a multi-dimensional integral which, in many cases, can be challenging or even impossible to evaluate. Fortunately, for many engineering applications, the detailed evaluation of the collision operator can be avoided by utilizing simplifying approximations such as the relaxation-time or BGK model, as first proposed by Bhatnagar *et al.*<sup>27</sup> In the relaxation-time model, the collision operator is represented by a source term of the form

$$\frac{\delta \mathcal{F}}{\delta t} = -\frac{1}{\tau} (\mathcal{F} - \mathcal{M}), \quad (9)$$

where  $\mathcal{M}$  is the Maxwell-Boltzmann distribution, the equilibrium solution to the Boltzmann equation towards which the non-equilibrium solution is relaxing, and  $\tau$  is a characteristic relaxation time for the collision processes. The relaxation time can be related to the Knudsen number,  $\text{Kn}$ , and a reference length scale,  $\ell$ , using  $\text{Kn} = \lambda/\ell$  and  $v_{\text{th}} = \lambda/\tau$  where  $v_{\text{th}}$  is the mean or thermal speed of the particles and  $\lambda$  is the mean free path travelled by the particles between collisions. Thus,

$$\tau = \frac{\lambda}{v_{\text{th}}} = \frac{\text{Kn} \ell}{v_{\text{th}}}, \quad (10)$$

showing that the relaxation time scales directly with Knudsen number.

The BGK operator of Eq. (9) is phenomenological in nature and provides only an approximation to the Boltzmann collision integral that ignores many of the details of inter-particle interactions. Nevertheless, it retains a number of the key qualitative and quantitative features of the true collision integral. In particular, the relaxation-time approximation preserves the usual collisional invariants and can be shown to satisfy Boltzmann's H theorem. Under equilibrium conditions ( $\text{Kn} \rightarrow 0$  and  $\tau \rightarrow 0$ ), it dictates that  $\delta \mathcal{F}/\delta t = 0$  and  $\mathcal{F} = \mathcal{M}$  as required. For collisionless flows ( $\text{Kn} \rightarrow \infty$  and  $\tau \rightarrow \infty$ ), the time scales of interest are much smaller than  $\tau$  and  $\delta \mathcal{F}/\delta t \approx 0$ , also as expected. The parameter  $\tau$  can also be chosen such that the correct continuum viscosity of the gas is predicted. In this case,

$$\tau = \frac{\mu}{p}, \quad (11)$$

where  $\mu$  is the fluid viscosity.

### D. Ellipsoidal Statistical Collision Operator

A well-known limitation of the BGK model, however, is that the collision operator always yields a Prandtl number,  $\text{Pr}$ , of one or greater. This result is in contradiction with physical expectations for Prandtl numbers for most gases, which tend to be less than unity.

Physically correct values of the Prandtl number are particularly important for accurate representation of heat transfer, which is the focus here. Fortunately, there are several other approximate collision operators available which can provide more realistic values of the Prandtl number. In the present work, an approximate collision term first proposed by Holway<sup>28</sup> will be used to describe collisional processes for monatomic gases. This collision operator, often referred to the ellipsoidal statistical model, preserves much of the simplicity of the BGK or relaxation-time model, while allowing for a realistic and selectable Prandtl number.

For a monatomic gas, the ellipsoidal statistical collision operator can be written as

$$\frac{\delta \mathcal{F}}{\delta t} = -\frac{1}{\tau_{\text{ES}}} (\mathcal{F} - \mathcal{G}_{\text{ES}}), \quad (12)$$

where

$$\mathcal{G}_{\text{ES}}(t, x_i, c_i) = \frac{(\rho/m)}{(2\pi)^{3/2} (\det \mathbf{T})^{1/2}} \exp\left(-\frac{1}{2} T_{ij}^{-1} c_i c_j\right). \quad (13)$$

It will be shown in the next sub-section that this distribution is a Gaussian distribution function that possesses a modified pressure tensor. The second-order tensor,  $T_{ij}$ , is defined to have the form

$$T_{ij} = (1 - \nu) \frac{p}{\rho} \delta_{ij} + \nu \Theta_{ij} = (1 - \nu) \frac{p}{\rho} \delta_{ij} + \nu \frac{P_{ij}}{\rho}, \quad (14)$$

where  $\Theta_{ij}$  is a symmetric ‘temperature’ tensor given by  $\Theta_{ij} = P_{ij}/\rho$  and  $P_{ij}$  is again the generalized pressure tensor. For monatomic gases, the ellipsoidal statistical collision model’s adherence to Boltzmann’s H theorem was first demonstrated by Andries and Perthame.<sup>29</sup> Andries *et al.*<sup>30</sup> have also considered extensions of the ellipsoidal statistical collision model to both diatomic and polyatomic gases and demonstrated that these extensions also satisfy the H theorem.

If the parameters  $\tau_{\text{ES}}$  and  $\nu$  associated with the ellipsoidal collision operator are chosen such that

$$\tau_{\text{ES}} = (1 - \nu)\frac{\mu}{p} = (1 - \nu)\tau, \quad 1 - \nu = \frac{1}{\text{Pr}}, \quad (15)$$

then the model will predict the correct values for fluid viscosity and thermal conductivity in the continuum limit. It is important to note that the relaxation times for the relaxation-time BGK and ellipsoidal statistical models,  $\tau$  and  $\tau_{\text{ES}}$ , differ by just a factor of the Prandtl number (i.e.,  $\tau_{\text{ES}} = \tau/\text{Pr}$ ). The moment equations and analyses to follow will be written in terms of the relaxation time for the standard BGK model,  $\tau$ , and Prandtl number,  $\text{Pr}$ , for consistency with traditional forms of these equations and other previous analyses.

### E. Maximum-Entropy Gaussian Closure for a Monatomic Gas

As discussed in the introduction, the lowest-order member of the maximum-entropy closure hierarchy of Levermore, other than the local-equilibrium Maxwellian closure leading to the Euler equations of compressible gas dynamics, is the 10-moment or Gaussian closure.<sup>5</sup> For a monatomic gas, the closure is constructed by considering the following set of velocity weights:

$$\mathbf{M}(v_\alpha) = [m, mv_i, mv_iv_j]^T, \quad (16)$$

corresponding to the macroscopic moments:

$$\langle \mathbf{M}(v_\alpha) \mathcal{F} \rangle = [\rho, \rho u_i, \rho u_i u_j + P_{ij}]^T. \quad (17)$$

Solution of the entropy-maximization problem for this set of moments is possible by analytical means and results in the following closed-form expression for the assumed form of the distribution function, the Gaussian distribution,  $\mathcal{G}$ , given by

$$\mathcal{F}(t, x_i, c_i) = \mathcal{G}(t, x_i, c_i) = \frac{(\rho/m)}{(2\pi)^{3/2} (\det \Theta)^{1/2}} \exp\left(-\frac{1}{2} \Theta_{ij}^{-1} c_i c_j\right), \quad (18)$$

where  $\Theta_{ij} = P_{ij}/\rho$  is an anisotropic ‘‘temperature’’ tensor. The Gaussian distribution appears to have been first derived in early work by Maxwell<sup>6</sup> and then re-discovered in subsequent but independent research by both Schlüter<sup>31,32</sup> and Holway.<sup>28,33–35</sup> It may be regarded as a generalization of the bi- and tri-Maxwellian velocity distribution functions with a form that does not require the identification of the planes of principal stress.<sup>31,32,36,37</sup> This approximate non-equilibrium distribution possesses a Gaussian-like distribution in each of the principal strain axes. Physically, it corresponds to a non-equilibrium condition with a different temperature in each direction.

The moment equations arising from the Gaussian closure for a monatomic gas can be obtained by taking  $\mathcal{F} = \mathcal{G}$ , using the ellipsoidal statistical approximation for the collision operator as proposed by Holway,<sup>28</sup> and substituting the velocity weights of Eq. (16) into Maxwell’s equation of change given by Eq. (8). This results in a strictly hyperbolic set of macroscopic transport equations which, in addition to balance equations for the gas density,  $\rho$ , and momentum,  $\rho u_i$ , contain transport equations for the symmetric non-equilibrium total flow energy tensor,  $\rho u_i u_j + P_{ij}$ . These hyperbolic moment equations can be summarized as follows:

$$\frac{\partial}{\partial t} (\rho) + \frac{\partial}{\partial x_i} (\rho u_i) = 0, \quad (19)$$

$$\frac{\partial}{\partial t} (\rho u_i) + \frac{\partial}{\partial x_j} (\rho u_i u_j + P_{ij}) = 0, \quad (20)$$

$$\frac{\partial}{\partial t} (\rho u_i u_j + P_{ij}) + \frac{\partial}{\partial x_k} (\rho u_i u_j u_k + u_i P_{jk} + u_j P_{ik} + u_k P_{ij}) = -\frac{1}{\tau} (P_{ij} - p\delta_{ij}). \quad (21)$$

Brown *et al.*,<sup>38,39</sup> have examined the eigenstructure and dispersive wave structure of the Gaussian closure, demonstrated the strict hyperbolicity of the moment equations, and developed an approximate Riemann solver for the closure for use in numerical solution methods based on a Roe linearization.<sup>40</sup>

It is noted that the closing fluxes in the Gaussian model involve third-order velocity moments. The construction of this second-order maximum-entropy closure is such that all third-order velocity moments are zero or

$$Q_{ijk} = \langle mc_i c_j c_k \mathcal{G} \rangle = 0, \quad q_i = \frac{1}{2} \langle mc_i c_j c_j \mathcal{G} \rangle = 0, \quad (22)$$

where  $Q_{ijk}$  is the third-order generalized heat flux tensor and  $q_i$  is the usual fluid-dynamic heat flux vector. These results point to the main limitation of the Gaussian closure: its inability to account for the effects of thermal diffusion. The primary objective of the regularization procedure considered herein is to remedy this situation.

## F. Maximum-Entropy Gaussian Closure for a Diatomic Gas

The preceding description is valid for a monatomic gas having no internal degrees of freedom or energy modes. An extension to the standard Gaussian closure for monatomic gases, that allows for the treatment of diatomic gases, was proposed previously by Hittinger<sup>13</sup> and has been studied by McDonald and Groth.<sup>10,20,41-44</sup> A similar extension that allows for the treatment of polyatomic gases has also been proposed by Le Tallec.<sup>45</sup> The diatomic extension of Hittinger is further modified here to allow for realistic values for the Prandtl number by making use of the ellipsoidal statistical collision operator introduced above. The proposed three-scale, relaxation-time, approximation for the collision operator is similar in many respects to the diatomic and polyatomic extensions of the ellipsoidal statistical model proposed by Andries *et al.*<sup>30</sup> and is described below.

The Gaussian closure for a diatomic gas is formulated by considering a generalization of the Boltzmann kinetic equation based on a classical treatment of the rotational degrees of freedom in which the molecules of the gas are treated as rigid bodies rotating about a translating center of mass whose net or total contributions to the average angular momentum of the gas by the internal modes is taken to be zero (i.e., the angular momentum of the rotational modes is a collisional invariant with a value of zero). It is also assumed that external forces and/or torques do not affect directly the internal rotational modes and that the microscopic molecular state of the particles is independent of their rotational orientation. The proposed treatment is then very similar to the fully classical treatments proposed by Bryan,<sup>46,47</sup> Pidduck,<sup>48</sup> Curtiss,<sup>49</sup> and Taxman<sup>50</sup> and is quite analogous to the semi-classical treatments proposed independently by Wang Chang and Uhlenbeck and de Boer.<sup>47,51</sup> The basic form of the kinetic equation as given in Eq. (1) is assumed to remain essentially unchanged for the diatomic case, except that the general non-equilibrium solution,  $\mathcal{F}$ , now depends on an enhanced set of independent variables,  $(t, x_i, c_i, \omega_\alpha)$ , which additionally includes the angular velocity vector of the molecule,  $\omega_\alpha$ , and the collision integral or operator must be appropriately modified. In the case of the Gaussian closure, the maximum-entropy velocity probability-density function is taken to have the form

$$\mathcal{G}_D(t, x_i, c_i, \omega_\alpha) = \frac{(\rho/m)(I/m)}{(2\pi)^{5/2} (\det \Theta)^{1/2} (p/\rho) (T_r/T)} \exp \left[ -\frac{1}{2} \left( \Theta_{ij}^{-1} c_i c_j + R_{\alpha\beta}^{-1} \omega_\alpha \omega_\beta \right) \right], \quad (23)$$

where  $I$  is the moment of inertia of a diatomic molecule,  $p$  is again the usual thermodynamic pressure,  $T$  is now the temperature associated with the translational energy,  $T_r$  is the rotational temperature, and

$$R_{\alpha\beta} = \left( \frac{mp}{I\rho} \right) \left( \frac{T_r}{T} \right) \delta_{\alpha\beta} = \left( \frac{me_r}{I} \right) \delta_{\alpha\beta}. \quad (24)$$

The specific rotational energy of the gas,  $e_r$ , is then given by  $e_r = (p/\rho)(T_r/T)$ . In the case of diatomic molecule,  $\omega_\alpha$  has just two non-vanishing components.

As for a monatomic gas, macroscopic properties of a general non-equilibrium distribution function,  $\mathcal{F}(t, x_i, c_i, \omega_\alpha)$ , representing a diatomic gas can be obtained by taking appropriate moments. In this case, the weight,  $M(v_i, \omega_\alpha)$ , is most generally a function of both the translational velocity,  $v_i$  and rotational velocity,  $\omega_\alpha$ , and moments can be defined as

$$\langle M(v_i, \omega_\alpha) \mathcal{F} \rangle = \int_{-\infty}^{\infty} M(v_i, \omega_\alpha) \mathcal{F}(t, x_i, v_i, \omega_\alpha) d^3v d^2\omega, \quad (25)$$

and require an integration over five dimensional space. In particular, for  $\mathcal{F} = \mathcal{G}_D$  as given by Eq. (23) above and for  $M(v_i, \omega_\alpha) = m$ ,  $I\omega_\alpha\omega_\beta$ , and  $I\omega^2/2$ , one can obtain

$$\int_{-\infty}^{\infty} m\mathcal{G}_D(t, x_i, v_i, \omega_\alpha) d^3v d^2\omega = \langle m\mathcal{G}_D \rangle = \rho(t, x_i), \quad (26)$$

$$\int_{-\infty}^{\infty} I\omega_\alpha\omega_\beta\mathcal{G}_D(t, x_i, v_i, \omega_\delta) d^3v d^2\omega = \langle I\omega_\alpha\omega_\beta\mathcal{G}_D \rangle = p\left(\frac{T_r}{T}\right)\delta_{\alpha\beta} = \rho(t, x_i)e_r(t, x_i)\delta_{\alpha\beta}, \quad (27)$$

$$\int_{-\infty}^{\infty} \frac{I}{2}\omega^2\mathcal{G}_D(t, x_i, v_i, \omega_\alpha) d^3v d^2\omega = \left\langle \frac{I}{2}\omega^2\mathcal{G}_D \right\rangle = \rho(t, x_i) = p\left(\frac{T_r}{T}\right) = \rho(t, x_i)e_r(t, x_i), \quad (28)$$

respectively.

For the purposes of deriving the moment equations of the diatomic Gaussian closure, a modified relaxation-time approximation for the collision operator is used herein similar to those proposed by Hittinger<sup>13</sup> and Andries *et al.*<sup>30</sup> The proposed collision model representing inter-particle collisions allows for three distinct time scales to be incorporated into the approximate collision operator: (i) the time scale for the relaxation of the energy of the translational motion of the particles to its equilibrium value; (ii) the time scale for the relaxation of translational energy; and (iii) a third time scale associated with relaxation processes for heat transfer, with the latter providing physically realistic values of the Prandtl number. This three-scale relaxation-time model takes the form

$$\frac{\delta\mathcal{F}}{\delta t} = -\frac{1}{\tau_t}(\mathcal{F} - \mathcal{G}_{ID}) - \frac{1}{\tau_r}(\mathcal{G}_{ID} - \mathcal{G}_{ESD}), \quad (29)$$

where it is assumed that the general non-equilibrium distribution relaxes first toward an intermediate ellipsoidal Gaussian distribution,  $\mathcal{G}_{ID}$ , for which the translational degrees of freedom are not at all in equilibrium with the rotational degrees of freedom, and then subsequently toward the modified ellipsoidal distribution function for the case of a diatomic gas,  $\mathcal{G}_{ESD}$ , for which the translational modes are now in partial equilibrium with the rotational modes.

The proposed three-scale collision model allows for the diatomic gas to have different relaxation times for the translational and rotational modes where, in Eq. (29),  $\tau_t$  and  $\tau_r$  are relaxation times associated with the translational and rotational degrees of freedom, respectively. As for the ellipsoidal statistical collision operator for a monatomic gas, simple approximate expressions can again be used to relate the relaxation times here to the appropriate gas viscosities and Prandtl number,  $Pr$ , as follows:

$$\tau_t = (1 - \nu)\frac{\mu}{p} = (1 - \nu)\tau, \quad \tau_r = (1 - \nu)\frac{15\mu_v}{4p} = (1 - \nu)\tau_v, \quad 1 - \nu = \frac{1}{Pr}, \quad (30)$$

where  $\mu$  is the fluid viscosity,  $\mu_v$  is the bulk or volume viscosity, and  $\tau_v = 15\mu_v/4p$ . Standard empirical relations can then be used to evaluate the viscosities. Generally,  $\tau_r$  and hence  $\tau_v$  are larger than, but of the same order of magnitude as,  $\tau_t$  and  $\tau$ . The three-scale, relaxation-time, collision model also satisfies the Boltzmann H theorem as is shown below.

Using the kinetic equation of Eq. (1) and the three-scale relaxation-time approximation defined above, the moment equations of the maximum-entropy Gaussian closure for a diatomic gas can thus be obtained by substituting appropriate weights into Maxwell's equation of change yielding

$$\frac{\partial}{\partial t}(\rho) + \frac{\partial}{\partial x_i}(\rho u_i) = 0, \quad (31)$$

$$\frac{\partial}{\partial t}(\rho u_i) + \frac{\partial}{\partial x_j}(\rho u_i u_j + P_{ij}) = 0, \quad (32)$$

$$\begin{aligned} \frac{\partial}{\partial t}(\rho u_i u_j + P_{ij}) + \frac{\partial}{\partial x_k}(\rho u_i u_j u_k + u_i P_{jk} + u_j P_{ik} + u_k P_{ij}) \\ = -\frac{1}{\tau}\left(P_{ij} - \frac{P_{kk}}{3}\delta_{ij}\right) - \frac{2}{15\tau_v}(P_{kk} - 3\rho e_r)\delta_{ij}, \end{aligned} \quad (33)$$

$$\frac{\partial}{\partial t}(\rho e_r) + \frac{\partial}{\partial x_i}(\rho u_i e_r) = -\frac{1}{5\tau_v}(3\rho e_r - P_{kk}), \quad (34)$$

As with the monatomic closure, the moment equations of the diatomic closure are also strictly hyperbolic and do not incorporate a description of heat transfer and predicts zero heat flux.



## G. Regularized Gaussian Closure

The regularized Gaussian closures were first introduced by McDonald and Groth<sup>11,12</sup> as an alternative to including heat transfer effects into the standard Gaussian closure. A more rigorous presentation of the material with full derivations is found in a subsequent publication by the authors,<sup>44</sup> complete with their application for two-dimensional flows. The regularization procedure for both monatomic and diatomic gases described here is based on that description and is included here for the purposes of completeness.

As stated earlier, one of the major shortfalls of these two Gaussian closures is their inability to account for thermal diffusion and heat transfer. This is due to the second-order nature of the closures and their assumed forms of the distribution function. Nevertheless, by allowing small deviations from Gaussian distributions, the effects of non-equilibrium heat transfer can be re-introduced into the closures. This can be done by applying Chapman-Enskog-like perturbative expansion techniques to either the moment equations directly or to the original underlying kinetic equations with model collision operators. In either case, the original Gaussian closure solution is used as the base solution for the expansion techniques. Both of these techniques are detailed here for the monatomic and diatomic gas cases. They are shown to give rise to a non-equilibrium treatment for heat transfer that is directly dependent on the anisotropic pressure or temperature tensor and the elliptic nature of the added terms leads to smooth regularized solutions. Additionally, unlike other regularized closure techniques, the underlying first-order moment systems are strictly hyperbolic for all realizable moments.

### 1. Monatomic Gas Regularized Gaussian Closure: Moment Equations

The monatomic Gaussian moment equations given by Eqs. (19)–(21) above provide a description of  $\rho$ ,  $u_i$ , and  $P_{ij}$  assuming that  $Q_{ijk} = 0$ . However, for more general non-equilibrium solutions with  $\mathcal{F} \neq \mathcal{G}$  and  $Q_{ijk} \neq 0$ , the total and random velocity moments,  $\rho u_i u_j + P_{ij} = \langle m v_i v_j \mathcal{F} \rangle$  and  $P_{ij} = \langle m c_i c_j \mathcal{F} \rangle$ , can be shown to satisfy the transport equations<sup>26</sup>

$$\frac{\partial}{\partial t} (\rho u_i u_j + P_{ij}) + \frac{\partial}{\partial x_k} (\rho u_i u_j u_k + u_i P_{jk} + u_j P_{ik} + u_k P_{ij} + Q_{ijk}) = -\frac{1}{\tau} (P_{ij} - p \delta_{ij}) . \quad (35)$$

and

$$\frac{\partial P_{ij}}{\partial t} + \frac{\partial}{\partial x_k} (u_k P_{ij}) + P_{jk} \frac{\partial u_i}{\partial x_k} + P_{ik} \frac{\partial u_j}{\partial x_k} + \frac{\partial Q_{ijk}}{\partial x_k} = -\frac{1}{\tau} (P_{ij} - p \delta_{ij}) , \quad (36)$$

respectively, where here the ellipsoidal statistical collision operator of Eq. (12) has been used in the evaluation of the collision terms. Equation (35) is the so-called weak conservation form of the generalized energy equation and Eq. (36) is the so-called non-conservation or primitive form. The influence of the generalized heat flux (a third-order moment) on the time evolution of  $P_{ij}$  (a second-order moment) is readily apparent and setting this third-order tensor to be identically zero results in a transport equation for  $P_{ij}$  that is identical to that of the Gaussian model.

The general primitive form of the moment equation describing the transport of the generalized heat flux tensor,  $Q_{ijk} = \langle m c_i c_j c_k \mathcal{F} \rangle$ , can be similarly derived and written as<sup>26</sup>

$$\begin{aligned} \frac{\partial Q_{ijk}}{\partial t} &+ \frac{\partial}{\partial x_l} (u_l Q_{ijk}) + Q_{jkl} \frac{\partial u_i}{\partial x_l} + Q_{ikl} \frac{\partial u_j}{\partial x_l} + Q_{ijl} \frac{\partial u_k}{\partial x_l} + P_{kl} \frac{\partial}{\partial x_l} \left( \frac{P_{ij}}{\rho} \right) \\ &+ P_{jl} \frac{\partial}{\partial x_l} \left( \frac{P_{ik}}{\rho} \right) + P_{il} \frac{\partial}{\partial x_l} \left( \frac{P_{jk}}{\rho} \right) + \frac{\partial K_{ijkl}}{\partial x_l} = -\frac{1}{(1-\nu)\tau} Q_{ijk} = -\frac{\text{Pr}}{\tau} Q_{ijk} , \end{aligned} \quad (37)$$

where again the collision term of Holway<sup>28</sup> has been used. In the transport equation above, the fourth-order tensor,  $K_{ijkl}$ , defined by

$$K_{ijkl} = \langle m c_i c_j c_k c_l \mathcal{F} \rangle - \langle m c_i c_j c_k c_l \mathcal{G} \rangle = \langle m c_i c_j c_k c_l \mathcal{F} \rangle - \frac{1}{\rho} [P_{ij} P_{kl} + P_{ik} P_{jl} + P_{il} P_{jk}] , \quad (38)$$

has been introduced. This term represents the deviation of the general non-equilibrium fourth random-velocity moment from that predicted by the Gaussian closure.

The preceding transport equation for the generalized heat flux tensor,  $Q_{ijk}$ , of Eq. (37) and the expression of Eq. (38) for the fourth-order deviatoric tensor,  $K_{ijkl}$ , can be used in combination with a Chapman-Enskog-like perturbative expansion technique to arrive at a perturbed solution to the Gaussian for correcting the

transport equations of Eqs. (35) and Eq. (36) and that provides a non-zero first-order deviation for the heat flux tensor in terms of the lower-order moments. As with the perturbative expansion technique applied to the kinetic equation, the working assumption for the development of the perturbed solution is that  $(1 - \nu) \ll 1$  or  $\text{Pr} \gg 1$ . In this approach, the solutions for the generalized heat flux tensor,  $Q_{ijk}$ , and fourth-order deviatoric tensor,  $K_{ijkl}$ , satisfying Eqs. (37) and (38) are represented by the perturbative expansions

$$Q_{ijk} = Q_{ijk}^{(0)} + Q_{ijk}^{(1)} + Q_{ijk}^{(2)} + Q_{ijk}^{(3)} + \dots = Q_{ijk}^{(1)} + Q_{ijk}^{(2)} + Q_{ijk}^{(3)} + \dots, \quad (39)$$

and

$$K_{ijkl} = K_{ijkl}^{(0)} + K_{ijkl}^{(1)} + K_{ijkl}^{(2)} + K_{ijkl}^{(3)} + \dots = K_{ijkl}^{(1)} + K_{ijkl}^{(2)} + K_{ijkl}^{(3)} + \dots. \quad (40)$$

where again the superscript ( $n$ ) denotes the  $n$ -th order correction and by definition of the solution construction it is known that

$$Q_{ijk}^{(0)} = 0, \quad K_{ijkl}^{(0)} = 0. \quad (41)$$

As with the perturbative expansion technique applied to the kinetic equation, a formal smallness parameter,  $\epsilon$ , is again introduced to scale the solution and moment equations with the assumption that  $\epsilon \ll 1$ . The scaled solutions  $Q_{ijk}$  and  $K_{ijkl}$  are then taken to have the form

$$Q_{ijk} = \epsilon Q_{ijk}^{(1)} + \epsilon^2 Q_{ijk}^{(2)} + \epsilon^3 Q_{ijk}^{(3)} + \dots, \quad (42)$$

and

$$K_{ijkl} = \epsilon K_{ijkl}^{(1)} + \epsilon^2 K_{ijkl}^{(2)} + \epsilon^3 K_{ijkl}^{(3)} + \dots. \quad (43)$$

and satisfy the scaled third-order moment equation

$$\begin{aligned} \frac{\partial Q_{ijk}}{\partial t} + \frac{\partial}{\partial x_l} (u_l Q_{ijk}) + Q_{jkl} \frac{\partial u_i}{\partial x_l} + Q_{ikl} \frac{\partial u_j}{\partial x_l} + Q_{ijl} \frac{\partial u_k}{\partial x_l} + P_{kl} \frac{\partial}{\partial x_l} \left( \frac{P_{ij}}{\rho} \right) \\ + P_{jl} \frac{\partial}{\partial x_l} \left( \frac{P_{ik}}{\rho} \right) + P_{il} \frac{\partial}{\partial x_l} \left( \frac{P_{jk}}{\rho} \right) + \frac{\partial \mathcal{K}_{ijkl}}{\partial x_l} = -\frac{1}{(1 - \nu)\epsilon\tau} Q_{ijk}, \end{aligned} \quad (44)$$

The small parameter,  $\epsilon$ , has been introduced here in accordance with the assumption that deviations of the moment quantities from those predicted by the Gaussian closure (i.e.,  $Q_{ijk} = 0$  and  $K_{ijkl} = 0$ ) will be attenuated rapidly by collisional processes.

Substituting the expansion of Eqs. (42) and (43) into the scaled moment equation for  $Q_{ijk}$  of Eq. (44) and collecting terms of equal order in  $\epsilon$ , it is easy to see that, to zeroth-order in  $\epsilon$ , the moment equation is automatically satisfied as should be expected. To first-order in  $\epsilon$ , it can be seen that the first-order correction for the heat flux tensor,  $Q_{ijk}^{(1)}$ , must satisfy

$$\begin{aligned} Q_{ijk}^{(1)} &= -(1 - \nu)\tau \left[ P_{kl} \frac{\partial}{\partial x_l} \left( \frac{P_{ij}}{\rho} \right) + P_{jl} \frac{\partial}{\partial x_l} \left( \frac{P_{ik}}{\rho} \right) + P_{il} \frac{\partial}{\partial x_l} \left( \frac{P_{jk}}{\rho} \right) \right] \\ &= -\frac{\tau}{\text{Pr}} \left[ P_{kl} \frac{\partial}{\partial x_l} \left( \frac{P_{ij}}{\rho} \right) + P_{jl} \frac{\partial}{\partial x_l} \left( \frac{P_{ik}}{\rho} \right) + P_{il} \frac{\partial}{\partial x_l} \left( \frac{P_{jk}}{\rho} \right) \right]. \end{aligned} \quad (45)$$

Assuming that  $Q_{ijk} \approx Q_{ijk}^{(1)}$  where  $Q_{ijk}^{(1)}$  is given by Eq. (45) and introducing this first-order perturbed solution for the generalized heat flux tensor into the moment equations for the gas density,  $\rho$ , momentum,  $\rho u_i$ , and non-equilibrium energy tensor,  $\rho u_i u_j + P_{ij}$ , gives rise to the moment equations for the regularized Gaussian closure that can be summarized as

$$\frac{\partial}{\partial t} (\rho) + \frac{\partial}{\partial x_i} (\rho u_i) = 0, \quad (46)$$

$$\frac{\partial}{\partial t} (\rho u_i) + \frac{\partial}{\partial x_j} (\rho u_i u_j + P_{ij}) = 0, \quad (47)$$

$$\begin{aligned} \frac{\partial}{\partial t} (\rho u_i u_j + P_{ij}) + \frac{\partial}{\partial x_k} (\rho u_i u_j u_k + u_i P_{jk} + u_j P_{ik} + u_k P_{ij}) \\ = \frac{\partial}{\partial x_k} \left\{ \frac{\tau}{\text{Pr}} \left[ P_{kl} \frac{\partial}{\partial x_l} \left( \frac{P_{ij}}{\rho} \right) + P_{jl} \frac{\partial}{\partial x_l} \left( \frac{P_{ik}}{\rho} \right) + P_{il} \frac{\partial}{\partial x_l} \left( \frac{P_{jk}}{\rho} \right) \right] \right\} \\ - \frac{1}{\tau} (P_{ij} - p\delta_{ij}), \end{aligned} \quad (48)$$

where it is evident that the correction for  $Q_{ijk}$  brings an elliptic nature to the moment equations and introduces a dissipation term that regularizes the solutions.

## 2. Diatomic Gas Regularized Gaussian Closure: Moment Equations

In the diatomic case however,  $Q_{ijk}$  does not represent the full effect of heat transfer. It can also be shown that the moment equation describing non-equilibrium transport of the moment  $\rho e_r = \langle I\omega^2 \mathcal{F} \rangle$  has the general form

$$\frac{\partial}{\partial t} (\rho e_r) + \frac{\partial}{\partial x_i} (\rho u_i e_r + h_i) = -\frac{1}{5\tau_v} (3\rho e_r - P_{kk}), \quad (49)$$

where  $h_i$  is the heat flux vector associated with the rotational as defined by

$$h_i = \langle Ic_i \omega^2 \mathcal{F} \rangle, \quad (50)$$

and represents the transport of rotational energy of the particles by their random translational motion. A general weak-conservation form of the moment equation describing the transport of the moment,  $u_i e_r + h_i = \langle Iv_i \omega^2 \mathcal{F} \rangle$ , may also be derived and written as

$$\begin{aligned} \frac{\partial}{\partial t} (\rho u_i e_r + h_i) + \frac{\partial}{\partial x_j} (\rho u_i u_j e_r + u_i h_j + u_j h_i + P_{ij} e_r + r_{ij}) \\ = -\frac{1}{(1-\nu)\tau} h_i - \frac{1}{5\tau_v} u_i (3\rho e_r - P_{kk}), \end{aligned} \quad (51)$$

where the deviatoric second-order tensor,  $r_{ij}$ , can be defined and expressed as

$$r_{ij} = \langle Ic_i c_j \omega^2 \mathcal{F} \rangle - \langle Ic_i c_j \omega^2 \mathcal{G}_D \rangle = \langle Ic_i c_j \omega^2 \mathcal{F} \rangle - P_{ij} e_r, \quad (52)$$

and this tensor represents the flux of  $h_i$  produced by the random translation motion of the particles. A non-conservation form of the moment equation describing the non-equilibrium transport of  $h_i$  can also be found and written as

$$\frac{\partial h_i}{\partial t} + \frac{\partial}{\partial x_j} (u_j h_i) + h_j \frac{\partial u_i}{\partial x_j} + P_{ij} \frac{\partial e_r}{\partial x_j} + \frac{\partial r_{ij}}{\partial x_j} = -\frac{1}{(1-\nu)\tau} h_i = -\frac{\text{Pr}}{\tau} h_i. \quad (53)$$

The Gaussian solution for the diatomic gas as represented by  $\mathcal{F} = \mathcal{G}_D$  does not allow for heat transfer and predicts that both  $Q_{ijk}$  and  $h_i$  are zero. This will clearly not be the case for more general non-equilibrium transport with  $\mathcal{F} \neq \mathcal{G}_D$ .

A Chapman-Enskog-like perturbative expansion technique can again be applied to derive a perturbed solution correction for the Gaussian closure that provides non-zero first-order deviations for the heat flux tensor,  $Q_{ijk}$ , and heat flux vector,  $h_i$ , in terms of the appropriate lower-order moments. Once again, the working assumption for the development of the perturbed corrections is that  $(1-\nu) \ll 1$  or  $\text{Pr} \gg 1$ . In this approach, the quantities  $Q_{ijk}$ ,  $K_{ijkl}$ ,  $h_i$ , and  $r_{ij}$  are all represented by the scaled perturbative expansions, with  $Q_{ijk}$  and  $K_{ijkl}$  defined as they were in the monatomic case and

$$h_i = \epsilon h_i^{(1)} + \epsilon^2 h_i^{(2)} + \epsilon^3 h_i^{(3)} + \dots, \quad (54)$$

$$r_{ij} = \epsilon r_{ij}^{(1)} + \epsilon^2 r_{ij}^{(2)} + \epsilon^3 r_{ij}^{(3)} + \dots, \quad (55)$$

where, similarly, by definition

$$h_i^{(0)} = 0, \quad r_{ij}^{(0)} = 0, \quad (56)$$

and where the smallness parameter,  $\epsilon$ , is a measure of the closeness of  $1-\nu$  to zero. The scaled expansions for  $Q_{ijk}$ ,  $K_{ijkl}$ ,  $h_i$ , and  $r_{ij}$  must satisfy the scaled moment equations for  $Q_{ijk}$ , which takes the same form as the monatomic description given in Eq. (45), and an additional moment equation for  $h_i$  given by

$$\frac{\partial h_i}{\partial t} + \frac{\partial}{\partial x_j} (u_j h_i) + h_j \frac{\partial u_i}{\partial x_j} + P_{ij} \frac{\partial e_r}{\partial x_j} + \frac{\partial r_{ij}}{\partial x_j} = -\frac{1}{(1-\nu)\epsilon\tau} h_i. \quad (57)$$

Obviously, to zeroth-order in  $\epsilon$ , the scaled moment equations for  $Q_{ijk}$  and  $h_i$  are automatically satisfied by the expansions for  $Q_{ijk}$ ,  $K_{ijkl}$ ,  $h_i$ , and  $r_{ij}$ . However, to first-order in  $\epsilon$ ,  $Q_{ijk}^{(1)}$  and  $h_i^{(1)}$  are required to have the forms

$$Q_{ijk}^{(1)} = -\frac{\tau}{\text{Pr}} \left[ P_{kl} \frac{\partial}{\partial x_l} \left( \frac{P_{ij}}{\rho} \right) + P_{jl} \frac{\partial}{\partial x_l} \left( \frac{P_{ik}}{\rho} \right) + P_{il} \frac{\partial}{\partial x_l} \left( \frac{P_{jk}}{\rho} \right) \right], \quad (58)$$

and

$$h_i^{(1)} = -\frac{\tau}{\text{Pr}} P_{ij} \frac{\partial e_r}{\partial x_j}. \quad (59)$$

The first-order perturbed solution for generalized heat flux tensor,  $Q_{ijk}$ , associated with the flux of the translational energy by the translational motion, given by Eq. (58) is identical to the result obtained above for the monatomic gas. The additional first-order solution for  $h_i$  of Eq. (59) prescribes the heat flux of the particle rotational energy quite naturally in terms of its gradient.

A regularized closure is then obtained by assuming that  $Q_{ijk} \approx Q_{ijk}^{(1)}$  and  $h_i \approx h_i^{(1)}$  where  $Q_{ijk}^{(1)}$  and  $h_i^{(1)}$  are given by Eqs. (58) and (59) above. With the addition of these corrections for heat transfer arising from the first-order perturbed solution, the moment equations of the proposed regularized Gaussian closure for a diatomic gas can be summarized as follows:

$$\frac{\partial}{\partial t} (\rho) + \frac{\partial}{\partial x_i} (\rho u_i) = 0, \quad (60)$$

$$\frac{\partial}{\partial t} (\rho u_i) + \frac{\partial}{\partial x_j} (\rho u_i u_j + P_{ij}) = 0, \quad (61)$$

$$\begin{aligned} \frac{\partial}{\partial t} (\rho u_i u_j + P_{ij}) &+ \frac{\partial}{\partial x_k} (\rho u_i u_j u_k + u_i P_{jk} + u_j P_{ik} + u_k P_{ij}) \\ &= \frac{\partial}{\partial x_k} \left\{ \frac{\tau}{\text{Pr}} \left[ P_{kl} \frac{\partial}{\partial x_l} \left( \frac{P_{ij}}{\rho} \right) + P_{jl} \frac{\partial}{\partial x_l} \left( \frac{P_{ik}}{\rho} \right) + P_{il} \frac{\partial}{\partial x_l} \left( \frac{P_{jk}}{\rho} \right) \right] \right\} \\ &\quad - \frac{1}{\tau} \left( P_{ij} - \frac{P_{kk}}{3} \delta_{ij} \right) - \frac{2}{15\tau_v} (P_{kk} - 3\rho e_r) \delta_{ij}, \end{aligned} \quad (62)$$

$$\frac{\partial}{\partial t} (\rho e_r) + \frac{\partial}{\partial x_i} (\rho u_i e_r) = \frac{\partial}{\partial x_i} \left( \frac{\tau}{\text{Pr}} P_{ij} \frac{\partial e_r}{\partial x_j} \right) - \frac{1}{5\tau_v} (3\rho e_r - P_{kk}). \quad (63)$$

These equations provide an extended fluid-dynamic description for non-equilibrium transport of diatomic gases.

## H. Velocity and Temperature Slip Boundary Conditions

### 1. Solid-Wall Boundary Conditions

A simple solid-wall boundary condition is employed for all of the micro-scale flow problems considered in this study. While low-order velocity moment conditions such as mass and momentum conservation are obvious for this case, boundary conditions are needed for the second-order velocity moments related to the anisotropic pressure tensor governing shear stress at the wall. Macroscopic properties as described in Section B have been found from the Boltzmann equation by integrating the distribution through velocity space, and a similar method can be used here to find boundary conditions at the wall, except that the distribution function used is affected by the reflection and accommodation of particles coming from the wall.

By assuming the existence of a Knudsen layer at the wall next to the solid surface, the particles at the surface can be described as a combination of the distribution functions of incoming and reflected particles. A fully diffuse reflection is assumed for the reflected particles. The moments of the resulting combination of distribution functions then provides the solid-wall boundary conditions needed for the Gaussian closure. A similar approach for solid wall boundary conditions was used by McDonald and Groth in earlier studies of the Gaussian closure applied to two-dimensional micro-scale flows.<sup>10-12, 20, 44</sup>

A thin layer of particles at the surface of a solid wall will be affected by particles approaching the wall and by particles entering it from a reflection against the wall. In the computational scheme used here, wall boundaries are rotated into a common frame of reference for calculations, then rotated back into their

original configuration. This frame of reference positions the wall on the  $xz$ -plane with flow approaching the wall normally in the  $-x$  direction. The following work on the Knudsen layer distribution function will adopt this frame as an example. The distribution function of the Knudsen layer  $\mathcal{F}_{\text{Kn}}$  becomes a summation of the distribution functions of the incoming particles  $\mathcal{F}_-$  and the reflected particles  $\mathcal{F}_+$ . Particles interacting with the wall will be reflected as a combination of their incoming Gaussian distribution function and a Maxwellian function as a result of accommodating effects at the wall. Defining an accommodation coefficient  $\alpha$ , the distribution function of the Knudsen layer can be defined as

$$\mathcal{F}_{\text{Kn}} = \mathcal{F}_+ + \mathcal{F}_-, \quad (64)$$

where  $\mathcal{F}_+$  and  $\mathcal{F}_-$  are defined as

$$\mathcal{F}_- = \begin{cases} \mathcal{G}_e(v_x, v_y, v_z) & \text{for } v_y < 0, \\ 0 & \text{for } v_y > 0, \end{cases} \quad (65)$$

$$\mathcal{F}_+ = \begin{cases} \alpha \mathcal{M}_w(v_x, v_y, v_z) + (1 - \alpha) \mathcal{G}_e(v_x, -v_y, v_z) & \text{for } v_y > 0, \\ 0 & \text{for } v_y < 0, \end{cases} \quad (66)$$

where  $\mathcal{M}_w$  is the Maxwellian distribution describing particles accommodated by the wall, and  $\mathcal{G}$  is the non-equilibrium distribution of the incoming particles. By taking the velocity moments of this combined distribution, the macroscopic properties of the Knudsen layer can be found and used for the solid-wall boundary conditions.

The number of boundary conditions needed at the wall can be determined by how the eigenvalues behave. The normal component,  $u_x$ , of the bulk velocity at the wall can be assumed to be zero as the wall does not emit or accumulate particles and constitutes one set of boundary conditions. By setting  $u_x = 0$  and substituting into the computed eigenvalues of the system, a total of three waves enter the fluid regime ( $\lambda > 0$ ) and are associated with the acoustic and shear waves described by the right eigenvectors. This result suggests that additional boundary conditions for the shear pressures at the wall are required. Instituting these boundary conditions also guarantees that if there is no accommodation at the wall ( $\alpha = 0$ ), the Gaussian closure will correctly recover the zero wall shear stress predicted by the Euler equations. The integration of the velocity moments for the shear stress in the Knudsen layer using the combined distribution function (64) along with the normal bulk velocity conditions yields a set of boundary conditions which can be summarized as

$$\bar{u}_y = \frac{1}{m(n + \frac{\alpha}{2}(n_w - n))} \left( \rho(2 - \alpha) \left( \frac{u_y}{2} - \sqrt{\frac{P_{xy}}{2\pi\rho P_{xx}}} \right) + \frac{\rho_w \alpha u_{y_w}}{2} \right) \quad (67a)$$

$$\bar{u}_z = \frac{1}{m(n + \frac{\alpha}{2}(n_w - n))} \left( \rho(2 - \alpha) \left( \frac{u_z}{2} - \sqrt{\frac{P_{xz}}{2\pi\rho P_{xx}}} \right) + \frac{\rho_w \alpha u_{z_w}}{2} \right) \quad (67b)$$

$$u_{x \text{ Kn}} = 0, \quad P_{xy \text{ Kn}} = \alpha \left[ \frac{P_{xy}}{2} + \sqrt{\frac{\rho P_{xx}}{2\pi}} (u_y - \bar{u}_y) + \sqrt{\frac{\rho_w n_w k T_w}{2\pi}} (u_{y_w} - \bar{u}_y) \right] \quad (67c)$$

$$P_{xz \text{ Kn}} = \alpha \left[ \frac{P_{xz}}{2} + \sqrt{\frac{\rho P_{xx}}{2\pi}} (u_z - \bar{u}_z) + \sqrt{\frac{\rho_w n_w k T_w}{2\pi}} (u_{z_w} - \bar{u}_z) \right]. \quad (67d)$$

where  $u_{x \text{ Kn}}$ ,  $P_{xy \text{ Kn}}$  and  $P_{xz \text{ Kn}}$  represent the values of the velocity components and shear stress in the Knudsen layer and where all other macroscopic quantities are those of the incoming Gaussian distribution with the exception of  $n_w$ ,  $u_{y_w}$ ,  $u_{z_w}$  and  $T_w$ , which define the Maxwellian,  $\mathcal{M}_w$ , for accommodated particles. It can be seen that Eqs. (67c) and (67d) allow for “velocity slip” and finite shear at the wall and recover the correct “no-shear”, “full-velocity-slip” limit for specular reflection ( $\alpha = 0$ ).

## 2. Additional Boundary Conditions for Heat Flux

Temperature slip at wall boundaries is one of the most significant physical characteristics present in high Knudsen number flows. Boundary conditions used up till this point involves rotating the Knudsen layer boundary state and the first interior cell into the  $x$ -direction and performing a series of half-Maxwellian

integrations to find the appropriate velocity moments. However, temperature slip cannot be modeled with these boundary conditions alone even with the regularization procedure described in the previous section, as the heat flux becomes dependent only on the pressure gradients through the wall, creating a corresponding smooth transition in temperature at the wall.

A method of introducing temperature slip into the boundary conditions has been proposed by Smoluchowski<sup>52</sup> and implemented for the two-dimensional Gaussian closure by McDonald and Groth.<sup>11,20</sup> The Knudsen layer temperature  $T$  is adjusted such that

$$T = T_w + \Delta T_s = T_w + f_s \lambda \frac{\partial T}{\partial n_i}, \quad (68)$$

where  $T$  is the temperature of the fluid at the boundary or edge of the Knudsen layer,  $T_w$  is the temperature of the wall introduced earlier,  $\Delta T_s$  is the temperature slip across the Knudsen layer,  $n_i$  is the unit vector normal to the wall, and  $f_s$  is the slip distance factor given by the expression

$$f_s = \frac{10\pi}{16\text{Pr}} \left( \frac{2 - \alpha}{\alpha} \right) \frac{\gamma}{\gamma + 1}, \quad (69)$$

and where  $\alpha$  is a again thermal accommodation coefficient. This adjusted temperature is then inserted into the boundary conditions to calculate the corresponding pressure tensor and rotational energy in the Knudsen layer, which in turn is used to calculate the pressure gradients used in (45) and (58).

### III. Finite Volume Scheme with NKS Scheme

In this study, a parallel, implicit, AMR, finite-volume scheme is proposed and developed for the solution of the moment equations of the regularized Gaussian moment closure as described above for both monatomic and diatomic gases. For the three-dimensional flows of interest here, the finite-volume discretization is applied to multi-block body-fitted meshes with hexahedral volume elements. The multi-block mesh and spatial discretization procedure readily allow for the application of solution-directed block-based AMR as developed previously by Gao *et al.*<sup>21–23,53–55</sup> for three space dimensions. In this block-based AMR scheme, a flexible block-based hierarchical octree data structure is used to facilitate automatic, solution-directed, and local adaptation of the mesh according to physics-based refinement criteria. The local refinement and coarsening of the mesh is carried out by division and merging of solution blocks, respectively. In the proposed finite-volume procedure, the hyperbolic fluxes at cell boundaries will be evaluated using a Riemann-solver based flux function by Roe, though an HLLC solver is also implemented. A Newton-Krylov-Schwarz (NKS) algorithm implemented for two and three-dimensional Navier-Stokes equations by Charest, Groth and Gülder<sup>56</sup> and Northrup and Groth<sup>57</sup> is employed for steady-state solutions and unsteady solutions as well using a dual-time stepping method. The elliptic heat transfer terms are incorporated using the technique implemented by Gao<sup>22</sup> with a centrally-weighted method for cell face gradients described by Mathur and Murphy.<sup>58</sup> The multi-block, body-fitted, AMR and Newton schemes are well suited to the parallel implementation of the parallel implicit finite-volume AMR scheme on distributed-memory multi-processor architectures via domain decomposition. Because of the self-similar nature of the grid blocks, domain decomposition is achieved by simply distributing the blocks making up the computational mesh equally among available processors and/or processor cores, with more than one block permitted per core.

The NKS solution algorithm for the set of non-linear algebraic equations that result from the spatial and temporal discretization procedures uses Newton's method with a Krylov subspace approach for the solution of the linear system at each Newton step. An additive Schwarz preconditioner is used in the parallel implementation of the Krylov subspace method, and is fully compatible with the block-based AMR and domain decomposition procedure that is described above and used in the parallel implementation of the solution method.

The semi-discrete form of the governing equations used in the finite volume method form a coupled set of non-linear ordinary differential equations. However, steady-state solutions (the primary focus here), can be computed directly by solving the nonlinear algebraic equations such that the residual vector  $\mathbf{R}(\mathbf{U}) = 0$  using Newton's method. Given an estimate to the solution to  $\mathbf{R}(\mathbf{U}) = 0$  at iteration level  $n$ , the following system of linear equations can be solved in Newton's method to obtain an improved estimate for the solution

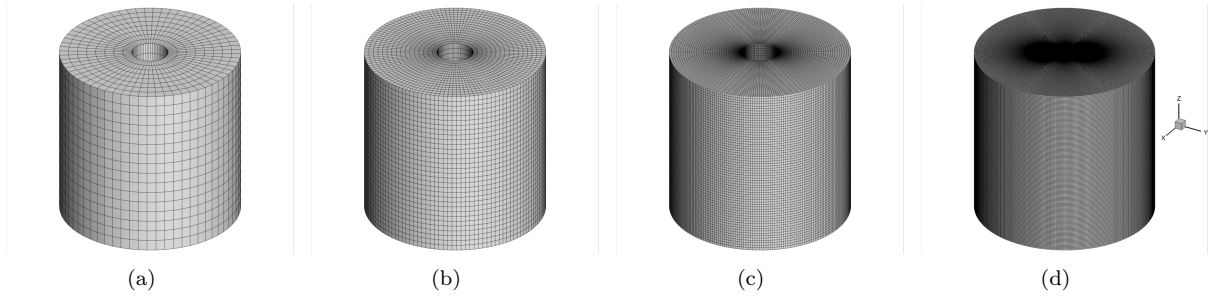


Figure 1. Manufactured solution grids generated from consecutive uniform mesh refinements.

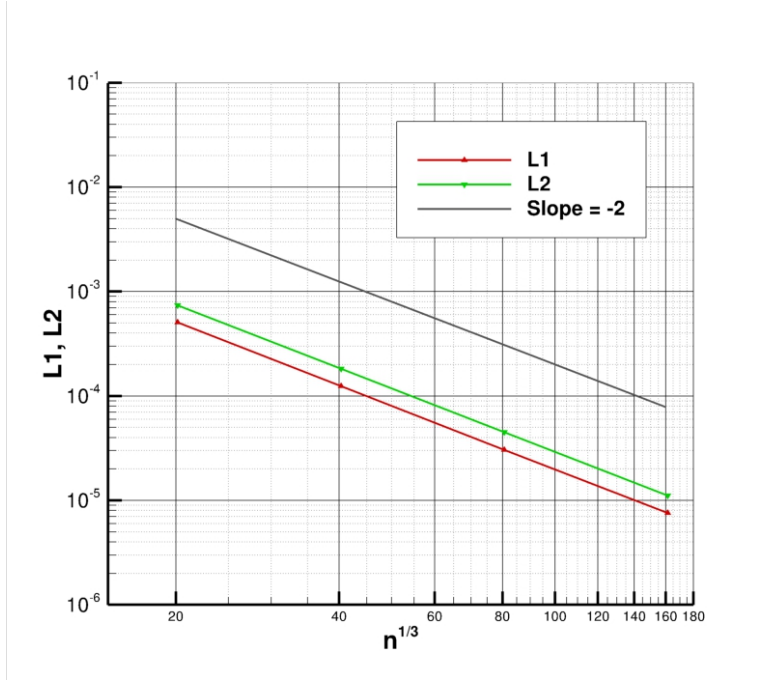


Figure 2.  $L_1$  and  $L_2$  error norms for the manufactured solution problem with increasing mesh densities.

at the  $n + 1$  iteration level,  $\mathbf{U}^{(n+1)}$ , satisfying  $\Delta\mathbf{U}^{(n+1)} = \mathbf{U}^{(n+1)} - \mathbf{U}^{(n)}$ :

$$\left(\frac{\partial \mathbf{R}}{\partial \mathbf{U}}\right)^{n+1} \Delta\mathbf{U}^{n+1} = \mathbf{J}\Delta\mathbf{U}^{n+1} \approx -\mathbf{R}(\mathbf{U}^{n+1}) \quad (70)$$

Given an initial estimate for the steady-state solution,  $\mathbf{U}^0$ , successively improved estimates for the solution  $\mathbf{U}^{n+1}$  are obtained by solving Equation (70) at each step,  $n$ , of the Newton method, where  $\mathbf{J} = \partial\mathbf{R}/\partial\mathbf{U}$  is the residual Jacobian. The iterative procedure is repeated until an appropriate norm of the solution residual is sufficiently small, i.e.,  $\|\mathbf{R}(\mathbf{U}^{(n+1)})\|_2 < \epsilon\|\mathbf{R}(\mathbf{U}^{(n)})\|_2$  where  $\epsilon$  is some small parameter (typically,  $\epsilon \approx 10^{-7}$ – $10^{-11}$ ).

Each step of Newton’s method requires the solution of a system of linear equations of the form  $\mathbf{J}\mathbf{x} = \mathbf{b}$ . This system is large, sparse, and non-symmetric and a preconditioned GMRES method<sup>59,60</sup> is used for its solution. In particular, a restarted version of the GMRES algorithm, GMRES( $m$ ), is used, where  $m$  is the number of steps after which the GMRES algorithm is restarted. Application of this iterative technique leads to an overall solution algorithm with iterations within iterations: the “inner loop” iterations involving the solution of the linear system and the “outer loop” iterations associated with the solution of the nonlinear problem. An inexact Newton method is adopted here in which the inner iterations are not fully converged

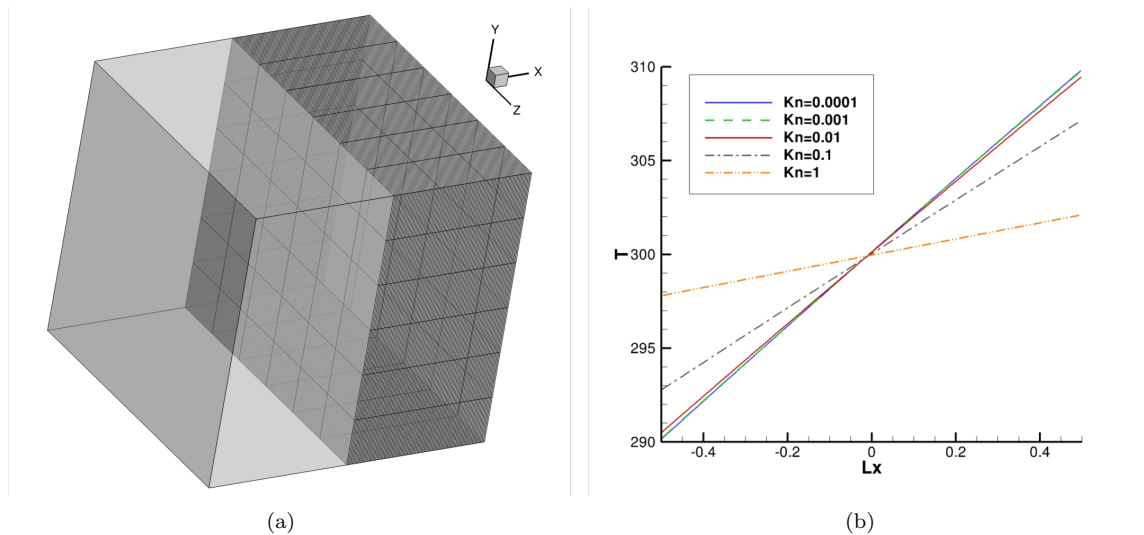


**Figure 3.** (a) A cutaway view of the two mesh blocks used for temperature profile calculations between two heated plates in the  $x$ -direction. (b) Temperature distribution between two isothermal walls over the non-dimensionalized wall separation distance  $L_x$  for a range of Knudsen numbers, with  $L_x = 0$  designating the centerline between the plates.

at each Newton step. The inner iterations are carried out only until  $\|\mathbf{R} + \mathbf{J}\Delta\mathbf{U}\|_2 \leq \zeta\|\mathbf{R}\|_2$ , where  $\zeta$  is typically in the range 0.01–0.5.

Preconditioning is required for the linear solver to be effective. Right preconditioning of the form  $(\mathbf{J}\mathbf{M}^{-1})(\mathbf{M}\mathbf{x}) = \mathbf{b}$  is used here where  $\mathbf{M}$  is the preconditioning matrix. An additive Schwarz global preconditioner with variable overlap<sup>60,61</sup> is used in conjunction with local preconditioners based on a block ILU( $f$ ) or BILU( $f$ ) factorization of an approximate Jacobian for each subdomain. Here,  $f$  is the level of fill. This combination of preconditioning fits well with the block-based AMR described by Northrup and Groth<sup>62</sup> and is compatible with domain decomposition methods, readily enabling parallel implementation of the overall Newton method. Rather efficient parallel implementations of implicit algorithms via Schwarz preconditioning have been developed by Keyes and co-researchers and successfully applied to the prediction of transonic full potential, low-Mach-number compressible combusting, and three-dimensional inviscid flows.<sup>61,63,64</sup>

As the GMRES algorithm does not explicitly require the evaluation of the global Jacobian matrix,  $\mathbf{J}$ , a so-called “matrix-free” or “Jacobian-free” approach can be adopted and is used here. Numerical differentiation based on Fréchet derivatives is used to approximate the matrix-vector product  $\mathbf{J}\mathbf{M}^{-1}\mathbf{x}$  as follows:

$$\mathbf{J}\mathbf{M}^{-1}\mathbf{x} \approx \frac{\mathbf{R}(\mathbf{U} + \varepsilon\mathbf{M}^{-1}\mathbf{x}) - \mathbf{R}(\mathbf{U})}{\varepsilon}, \quad (71)$$

where  $\mathbf{R}(\mathbf{U} + \varepsilon\mathbf{M}^{-1}\mathbf{x})$  is the residual vector evaluated at some perturbed solution state and  $\varepsilon$  is a small scalar quantity. Although the performance of the Jacobian-free method is sensitive to the choice of  $\varepsilon$ , Neilsen *et al.*<sup>65</sup> have found that  $\varepsilon = \varepsilon_o/\|\mathbf{x}\|_2^{1/2}$  seems to work well, with  $\varepsilon_o \approx 10^{-8}$ – $10^{-7}$ .

## IV. Numerical Results and Validation

The regularized Gaussian closure with an extended treatment for heat transfer has been applied to a number of three-dimensional problems outlined below. An analysis of the spatial accuracy of the scheme and the effectiveness of the NKS and AMR algorithms as applied to the the three dimensional regularized Gaussian closure is also demonstrated.

### A. Manufactured Solution

The finite-volume scheme employed for these flow problems is similar to those used in previous studies of the two-dimensional Gaussian closure by McDonald and Groth.<sup>10–12</sup> A spatial accuracy assessment for the



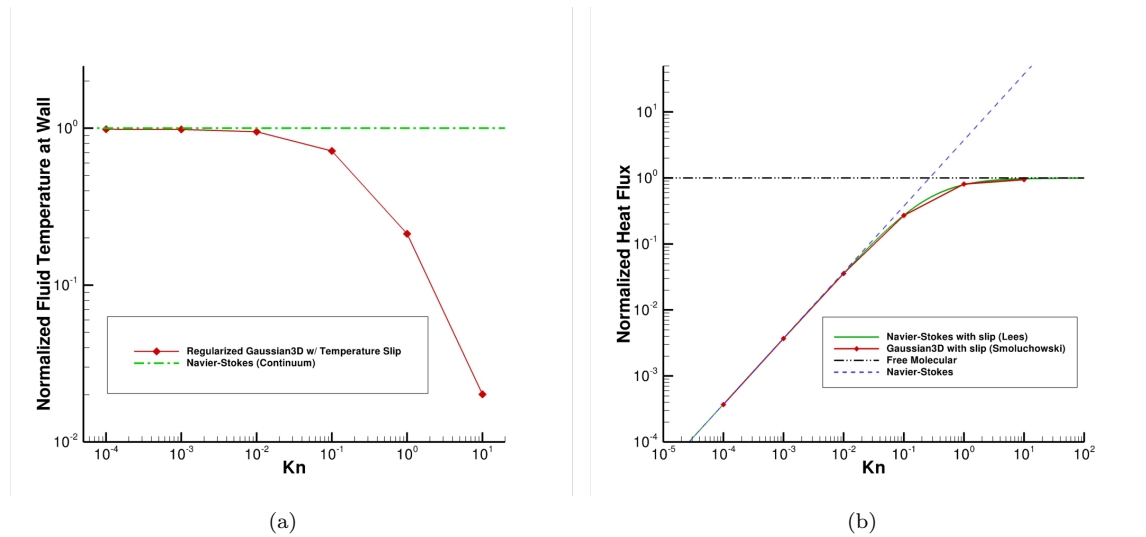


Figure 4. (a) Change in normalized temperature at the heated wall with increasing Knudsen number, (b) Heat flux between the plates normalized to the free-molecular solution.

same finite-volume scheme with the Euler equations has been performed by Sachdev and Groth,<sup>66,67</sup> and more recently for the two-dimensional Gaussian closure with embedded boundaries by McDonald *et al.*<sup>44</sup> As the second-order spatial accuracy of the scheme has been demonstrated for the moment equations of interest here, the task that remains is to demonstrate that the spatial accuracy is maintained for three-dimensional flows. As practical situations with exact analytical solutions for the three-dimensional Gaussian closure are not known at the present time, the accuracy of the proposed scheme is instead verified with the method of manufactured solutions.<sup>68</sup> This accuracy assessment mirrors closely the analysis carried out previously by McDonald *et al.*<sup>44</sup>

The method of manufactured solutions constructs a chosen analytical solution over the domain of interest and drives the PDEs of interest towards this solution through the addition of source terms. This chosen analytical solution for the Gaussian closure,  $\hat{\mathbf{U}}$ , can be used to determine its associated solution residual vector,  $\hat{\mathbf{R}}$ , based on a re-expression of Eqs. (60)–(63) in weak conservation form such that

$$\hat{\mathbf{R}} = \frac{\partial \hat{\mathbf{U}}}{\partial t} + \frac{\partial \mathbf{F}(\hat{\mathbf{U}})}{\partial x} + \frac{\partial \mathbf{G}(\hat{\mathbf{U}})}{\partial y} + \frac{\partial \mathbf{H}(\hat{\mathbf{U}})}{\partial z} - \mathbf{S}(\hat{\mathbf{U}}) \quad (72)$$

where  $\mathbf{F}$ ,  $\mathbf{G}$ , and  $\mathbf{H}$  are the flux vectors of the analytical solution in the  $x$ -,  $y$ -, and  $z$ - directions respectively, and  $\mathbf{S}$  is the associated source term. This residual vector is then added as a source term onto the original set of equations in the form

$$\frac{\partial \mathbf{U}}{\partial t} + \frac{\partial \mathbf{F}(\mathbf{U})}{\partial x} + \frac{\partial \mathbf{G}(\mathbf{U})}{\partial y} + \frac{\partial \mathbf{H}(\mathbf{U})}{\partial z} = \mathbf{S}(\mathbf{U}) + \hat{\mathbf{R}} \quad (73)$$

such that the computed solution vector,  $\mathbf{U}$ , is driven towards the prescribed solution,  $\hat{\mathbf{U}}$ , at the convergence limit. Spatial accuracy can then be evaluated by comparing this computed solution vector to the prescribed analytical solution.

Time-invariant solutions are found using the three-dimensional Gaussian closure for a monatomic gas between two concentric cylinders. The interior and exterior cylinder radii are 0.5 m and 1.0 m respectively,

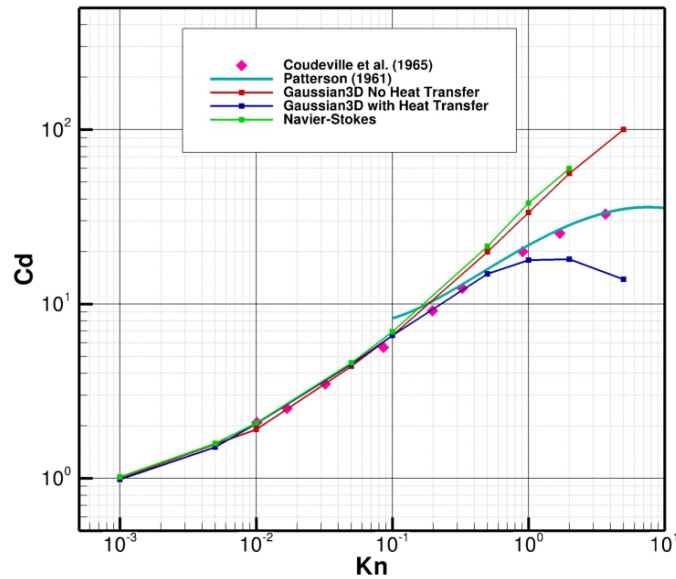


Figure 5. Drag coefficient over a cylinder vs. Knudsen number for a speed ratio  $S = 0.107$ .

with a cylinder height of 1.0 m. The prescribed solution for this analysis is given by

$$\begin{aligned}
 \rho &= 2 + \sin(x + y), \\
 u_x &= \cos(x + y), \\
 u_y &= \sin(x - y), \\
 u_z &= 0, \\
 P_{xx} &= 3 - \sin(x + y), \\
 P_{xy} &= \sin(y - x), \\
 P_{xz} &= 0, \\
 P_{yy} &= 3 + \cos(x + y), \\
 P_{yz} &= 0, \\
 P_{zz} &= 3 + \cos(-x - y),
 \end{aligned} \tag{74}$$

where the  $x$ - and  $y$ - axes lie within the plane of the circular base and the  $z$ -axis extends along the length of the cylinder as seen in Figure 1. Three consecutive uniform mesh refinements can also be seen in Figure 1 resulting in grids with 8,192, 65,536, 524,288 and 4,194,304 computational cells. Boundary conditions are fixed according to the prescribed analytical solution with reference to its position in three-dimensional space. The NKS algorithm developed for the solution of the three-dimensional Gaussian closure is used herein to find the time-invariant solution. The forcing nature of the manufactured residual source term towards the analytical solution and the simplified boundary conditions and flow conditions allows the NKS solution algorithm to reach ideal convergence rates, with  $L_2$ -norm residual reductions of up to 12 orders of magnitude.

The error norms between the computed solution and the analytical solution with increasing mesh resolution can be seen in Figure 2. The  $L_1$  and  $L_2$  norms are calculated using the difference between computed and analytical solution at each cell center and weighted according to the volume of the cell. The three-dimensional nature of the problem prompts a comparison to the nominal mesh density given by the cube root of total number of cells,  $n^{1/3}$ . A reference line with a slope of -2 is included for comparison, and clearly illustrates the second-order spatial accuracy of the scheme.

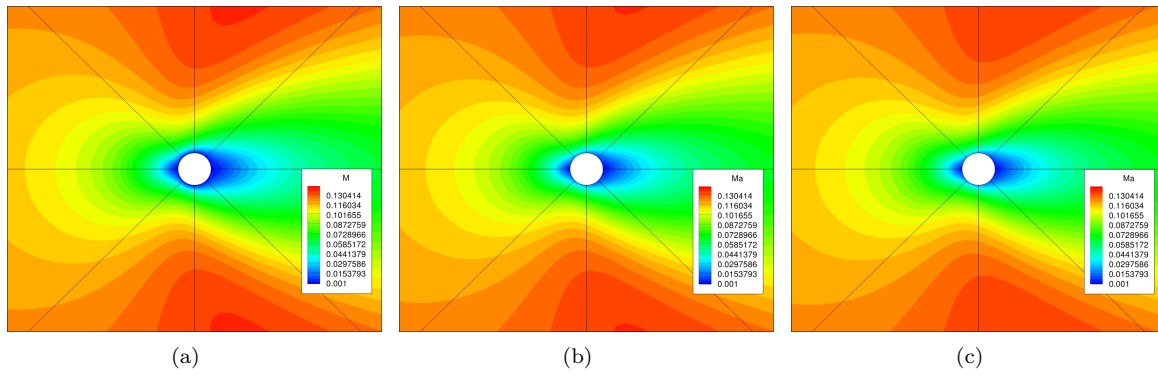


Figure 6. Mach number profile of flow over a cylinder at  $Kn=0.1$  as calculated by (a) Navier-Stokes, (b) standard Gaussian closure with no heat transfer, and (c) regularized Gaussian closure with heat transfer.

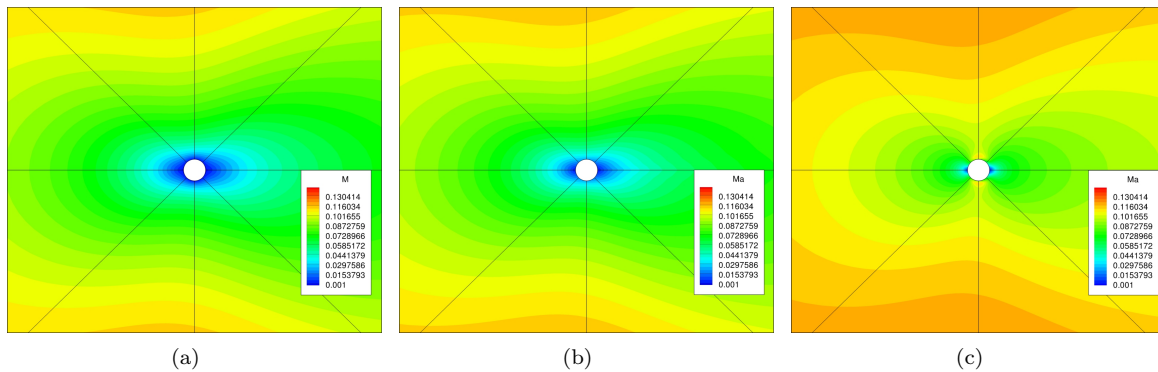


Figure 7. Mach number profile of flow over a cylinder at  $Kn=1.0$  as calculated by (a) Navier-Stokes, (b) standard Gaussian closure with no heat transfer, and (c) regularized Gaussian closure with heat transfer.

## B. Heated Plates

The regularized moment closures in combination with the slip flow boundary conditions described above have been used to model the temperature profile between two heated infinite plates over a wide range of Knudsen numbers. Argon initially at 300 K and standard pressure is placed between two isothermal plates oriented in the  $x$ -direction with  $T_L = 290$  K and  $T_R = 310$  K, separated by a distance ranging from  $7.05973 \times 10^{-4}$  to  $7.05973 \times 10^{-9}$  m corresponding to  $10^{-4} \leq Kn \leq 10$ . The computational mesh can be seen in Figure 3(a), and consists of 200 cells in the  $x$ -direction and 6 cells each in the transverse directions. The temperature profile between the plates is shown in Figure 3(b). The temperature slip phenomenon is clearly visible entering the transition regime at  $Kn = 10^{-1}$  and continues well into the free molecular regime. Figure 4 shows the calculated normalized wall temperature at the high temperature wall and the normalized heat flux calculated between the plates. In Figure 4(a), the temperature is normalized with the expression

$$T^* = \frac{T - T_m}{T_w - T_m} \quad (75)$$

where  $T^*$  is the normalized temperature,  $T_m$  is the temperature of the gas midway between the plates,  $T_w$  is the temperature of the wall, and  $T$  is the measured temperature of the gas at the wall. The figure clearly shows the temperature slip effect with increasing Knudsen number which is not captured by the Navier-Stokes. These results can be captured using the boundary conditions by Smoluchowski.<sup>52</sup> Figure 4(b) shows the variation of the normalized heat flux with increasing Knudsen number. The heat flux is normalized to

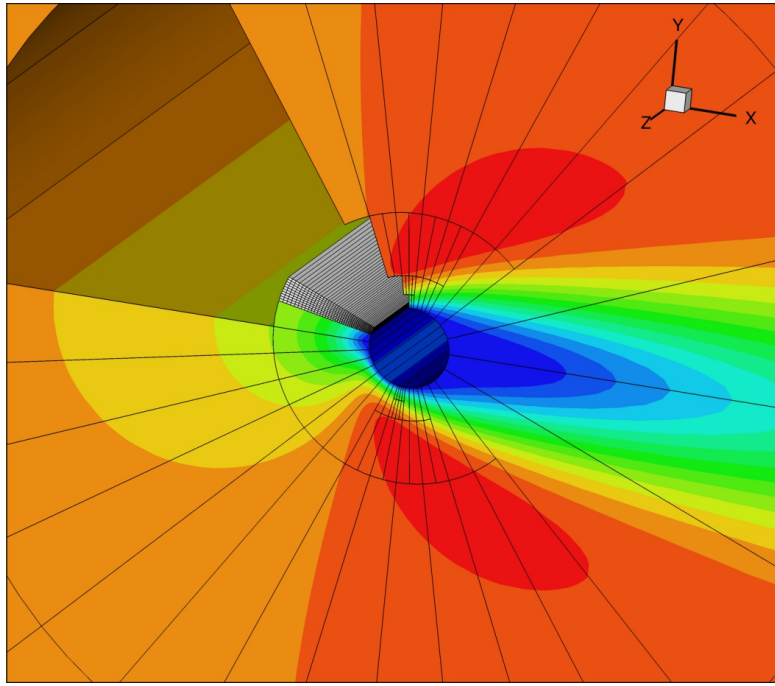


**Figure 8.** Mesh blocks created with the AMR algorithm for flow over a cylinder at  $\text{Kn} = 0.01$ . The uncolored block shows the individual cells residing within that particular mesh block to illustrate the resolution acquired.

the free molecular heat flux,  $q_{fm}$ , given by Bird<sup>1</sup> as

$$q_{fm} = -\rho(2R)^{\frac{3}{2}} \left( \frac{T_U T_L}{\pi} \right)^{\frac{1}{2}} \left( T_U^{\frac{1}{2}} - T_L^{\frac{1}{2}} \right) \quad (76)$$

where  $T_U$  and  $T_L$  are the temperatures of the upper and lower plate at 310 K and 290 K, respectively, and  $R$  is the specific gas constant. The Gaussian closure with temperature slip boundary conditions predicts a heat flux in line with those of the Navier-Stokes in the continuum limit, and smoothly transitions to the perfect temperature slip characterized by the free molecular limit with increasing Knudsen number.

### C. Flow Past an Immersed Cylinder with Heat Transfer

Immersed flow over a cylinder was studied here to observe the effects of heat transfer on drag coefficients over a range of Knudsen numbers, and can be compared to previous three-dimensional results for the Gaussian closure obtained by Lam and Groth<sup>69</sup> that did not include heat transfer. The proposed NKS solution method is employed to with the temperature slip boundary conditions of Smoluchowski.<sup>52</sup> Isothermal boundary conditions were used and set at a free stream temperature of 288 K. As a result, the heat flux from the wall into the fluid is not large and the temperature slip phenomena should manifest itself only in higher Knudsen number regimes.

The effects of laminar flow past a cylinder in both the continuum and transitional regimes has been studied experimentally by Coudeville *et al.*,<sup>70</sup> with focus on the drag coefficient with varying Reynolds and Knudsen numbers. For this study, the cylinder radii varies from  $3.36 \times 10^{-5}$  to  $6.72 \times 10^{-9}$  m, corresponding to  $10^{-3} \leq \text{Kn} \leq 5$ . A speed ratio of  $S = 0.107$  is used here and corresponds to a Mach number of  $\text{Ma} = 0.128$ , where the speed ratio is defined as the ratio between the bulk speed of the fluid and the most probable random speed of a particle. The Reynolds numbers for these flows ranges from  $0.005 \leq \text{Re} \leq 188$ , well within the laminar regime. The far field boundary was set at 32 times the cylinder radius, however, for  $\text{Kn} = 1 \times 10^{-1}$ , the boundary layer formed around the cylinder expands considerably, and the far field boundaries were extended up to 300 times the cylinder radius to avoid any interaction with the boundary layer. Final three-dimensional mesh resolution ranges from 83,200 to 166,400 cells.

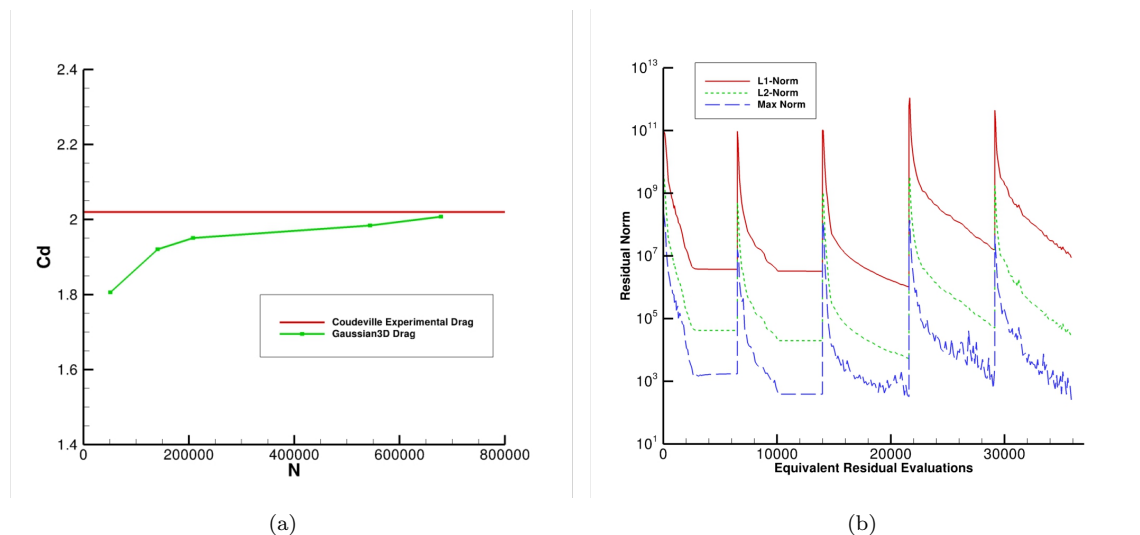


**Figure 9.** (a) Cylinder drag for  $Kn = 0.01$  with increasing number of cells, showing mesh-convergent behavior approaching the experimental data of Coudeville *et al.*,<sup>70</sup> (b) Error norm evolution over multiple mesh refinements.

A comparison can be made between the predictions of the Gaussian closure with and without heat transfer and the Navier-Stokes equations pertaining to the immersed flow over a cylinder with varying Knudsen number. Figure 5 shows the performance of these three descriptions compared to the experimental measurements by Coudeville *et al.*<sup>70</sup> and an analytical solution valid for the free molecular regime of Patterson.<sup>71</sup> The addition of heat transfer maintains physical accuracy up till about  $Kn = 1.0$  but drops off for higher Knudsen numbers. Interestingly, the Gaussian closure without heat transfer and the Navier-Stokes equations predict similar overestimated drag coefficients even though the Navier-Stokes model includes heat transfer, but not slip. To get a sense of the structure of the boundary layer predicted by these methods, the Mach number profiles for a transition regime problem ( $Kn = 0.1$ ) and free molecular regime problem ( $Kn = 1$ ) are shown in Figures 6 and 7, respectively. In the transition regime, all three methods produce similar drag coefficients and boundary layer thicknesses, but the lack of velocity slip at the cylinder boundaries in the Navier-Stokes is already evident. Adding heat transfer in the regularized Gaussian closure does not produce any noticeable effects at this point. At  $Kn = 1.0$ , the overestimation of the cylinder drag by the Navier-Stokes and the Gaussian closure without heat transfer can be related to an overestimation of the boundary layer thickness as evidenced by Figures 7(a) and 7(b). The addition of heat transfer in Figure 7(c) suppresses the growth of the boundary layer and results in a cylinder drag more in line with experimental and analytical data. However for  $Kn > 1$ , the suppressed boundary layer gives way to an underestimation of the drag which becomes worse with increasing  $Kn$ . This limit may represent a point at which the current form of the equations breaks down and can be also seen in the results of other moment techniques.<sup>72</sup> Further study into the physical phenomena occurring in this regime will be subject of future study.

It is useful at this point to illustrate the advantages in computational cost provided by the AMR and NKS algorithm for solutions to the three-dimensional Gaussian closure. For  $Kn = 0.01$ , the AMR algorithm was used to produce a cylinder mesh with up to four levels of refinement. A close-up view of the mesh blocks produced from the AMR procedure can be seen in Figure 8.

At each mesh refinement, the drag over the cylinder was calculated and compared to the experimental result from Coudeville *et al.*<sup>70</sup> for the same flow conditions. Figure 9(a) shows the mesh convergence of the solution method with reference to the calculated drag over the cylinder. The strength of the AMR/NKS solution method is even more pronounced as the converged computational drag approaches the experimental drag to within 0.6%. The convergence history of the NKS solution method with consecutive mesh refinements from the AMR algorithm can be seen in Figure 9(b), showing rapid convergence can be seen at each mesh level. The grid refinement is set to occur every 60 Newton iterations, though if allowed to proceed further the norm can be reduced by more than the approximately five orders of magnitude shown here.

The advantages offered by the NKS include a vast saving in computational costs. Figure 10 shows the

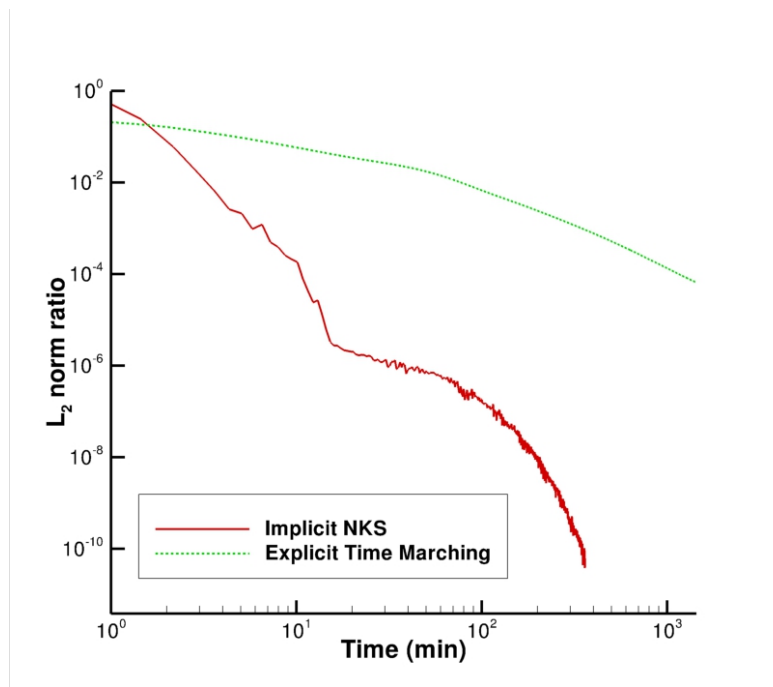


Figure 10. Convergence history for flow over a cylinder with respect to reduction of  $L_2$  density norms for  $\text{Kn} = 0.01$  using an explicit time marching scheme and the proposed implicit NKS solution method.

convergence history of the above-mentioned problem for measuring cylinder drag at  $\text{Kn} = 0.01$  with no AMR with a total of 179,200 cells. The explicit solver used for this evaluation has been previously described by McDonald and Groth<sup>10,11</sup> and used for the solution of the Gaussian closure without heat transfer by Lam and Groth.<sup>69</sup> Both schemes were performed over eight Intel Xeon E5540 cores at 2.53 GHz. As seen in the figure, for an equivalent drop of four orders of magnitude in the residual, the NKS scheme requires 10 minutes while the explicit method requires 48 hours, providing a reduction in the overall computational costs of the simulations by a factor of 100. The convergence history also shows that the NKS solution method is capable of reducing the residual by almost eleven orders of magnitude. The ability to reach a highly converged solution, the enormous savings in computational time, and the accuracy of the method shown in the examples above demonstrate that these moment closures can be readily used for both research and industrial applications.

#### D. Flow Past an Immersed Sphere

Non-equilibrium flow past a sphere is examined next. For the flow of interest, the sphere radius varies from  $3.36 \times 10^{-5}$  to  $6.72 \times 10^{-9}$  m, corresponding to a Knudsen number ranging from  $\text{Kn} = 10^{-3}$  to  $\text{Kn} = 5$ . The computed Gaussian closure solutions were obtained for air at 288 K at standard atmospheric pressure. The velocity and temperature slip boundary conditions were used in all cases. A cubed sphere grid consisting of 48 blocks with 25,600 cells per block for a grand total of 1,228,800 cells. The radius of the outer boundary is set to be 100 times the sphere radius, though this limit is expanded to accommodate the larger boundary layers as the Knudsen number increases. A sample of the cubed sphere grid blocks and a sample Mach number profile can be seen in Figure 11.

The predicted drag coefficient on a sphere in immersed flow is plotted against the Reynolds number in Figure 12. The numerical results are compared to the experimental results by Roos and Willmarth<sup>73</sup> and Liebster,<sup>74</sup> as well as with an analytical solution given by Flemmer and Banks.<sup>75</sup> The Reynolds number for these cases is altered through the effective diameter of the sphere while keeping all other parameters constant. Decreasing  $\text{Re}$  then corresponds to increasing  $\text{Kn}$ , reaching  $\text{Kn} = 1.0$  at  $\text{Re} = 0.1935$ . For smaller Reynolds numbers, the Gaussian closure begins to deviate from the analytical solution at about the same Knudsen number where a similar breakdown in drag prediction was seen in the above-described cylinder drag study.

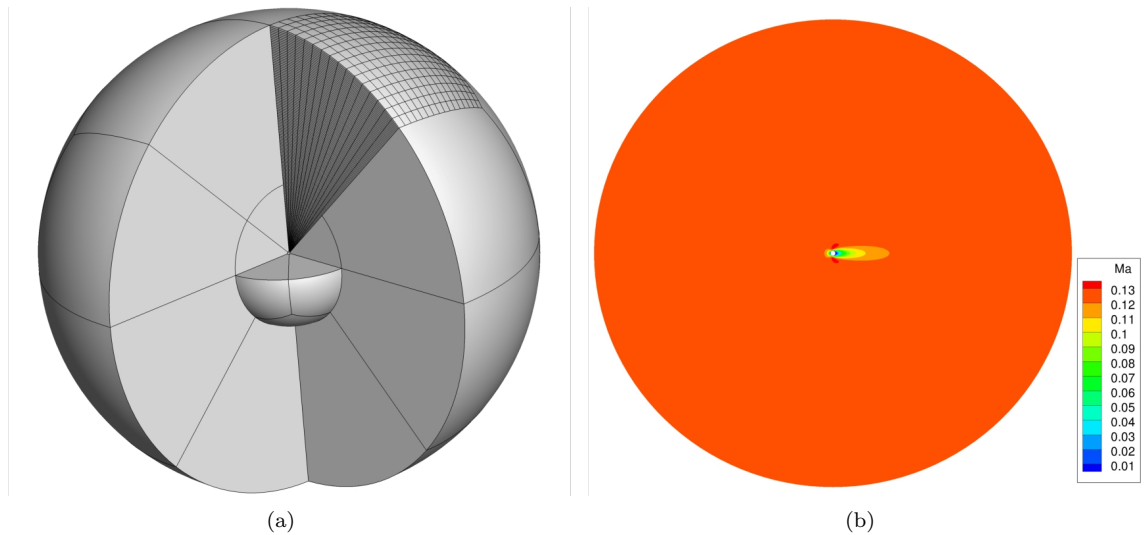


**Figure 11.** (a) A cutaway view of 6 mesh blocks for immersed flow over a sphere in the continuum regime with Mach number contours, (b) Sample result Mach number profile for  $Kn = 0.01$

It is important to note here that the Reynolds number for the experimental results was varied through the manipulation of the free stream flow, while the Gaussian closure results were performed with varying sphere diameters. While the use of non-dimensionalized parameters should negate any discrepancies in the overall comparison of the two sets of results, the performance of the Gaussian closure for low Reynolds numbers  $Re < 1$  also corresponds to a Knudsen number entering the free-molecular range where slip flow is taken into account. The analytical and experimental results were done in the continuum regime for these low Reynolds numbers and may account for their discrepancies with the Gaussian closure. Additional modifications to the analytical solution for low Reynolds numbers at high Knudsen numbers may be required, though the true behavior of the sphere drag coefficient is difficult to ascertain in the absence of relevant experimental data at this time.

## V. Conclusion

The numerical solution of the regularized Gaussian closure by means of a parallel, implicit, AMR, upwind, finite-volume scheme has been considered herein as an alternative for the simulation of micro-scale transition regime flows. While the inclusion of elliptic terms to the underlying strictly hyperbolic system of PDEs in the standard Gaussian closure may incur a higher computational cost, the ability to model heat transfer in the regularized system vastly outweighs this disadvantage. For the flow problems studied here, the regularized closures' ability to model non-equilibrium flows with velocity and temperature slip directly from kinetic theory is contrasted with the extensive modifications needed when using the Navier-Stokes equations. The relatively simple application of the parallel implicit NKS scheme for accelerated steady-state solutions makes the regularized Gaussian closure an attractive option both for academic and industrial purposes. Future work will involve extending the equation set further into the free molecular regime and a deeper investigation into the construction of slip boundary conditions.

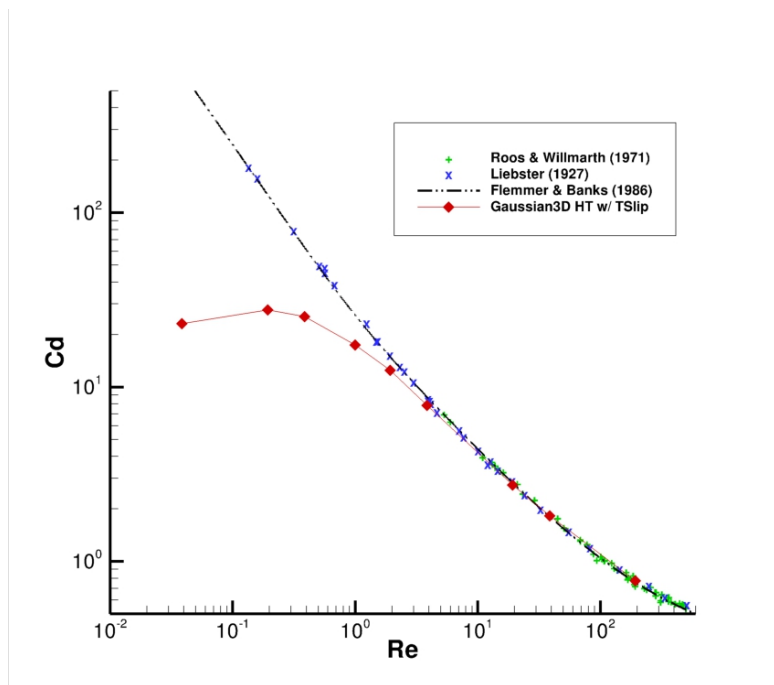


Figure 12. Drag coefficient over a sphere for varying Reynolds numbers: Gaussian closure vs. experimental and analytical results.

## References

- <sup>1</sup>Bird, G. A., *Molecular Gas Dynamics and the Direct Simulation of Gas Flows*, Clarendon Press, Oxford, 1994.
- <sup>2</sup>Hellman, A. N., Kaustubh, R. R., Yoon, H. H., Bae, S., Palmer, J. F., Phillips, K. S., Allbritton, N. L., and Venugopalan, V., "Laser-Induced Mixing in Microfluidic Channels," *Anal. Chem.*, Vol. 79, 2007, pp. 4484–4492.
- <sup>3</sup>de Divitiis, N., de Matteis, G., and de Socio, L. M., "Dynamics of Aerospace Vehicles at Very High Altitudes," *Meccanica*, Vol. 29, 1994, pp. 61–80.
- <sup>4</sup>Grad, H., "On the Kinetic Theory of Rarefied Gases," *Communications on Pure and Applied Mathematics*, Vol. 2, 1949, pp. 331–407.
- <sup>5</sup>Levermore, C. D., "Moment Closure Hierarchies for Kinetic Theories," *Journal of Statistical Physics*, Vol. 83, 1996, pp. 1021–1065.
- <sup>6</sup>Maxwell, J. C., "On the Dynamical Theory of Gases," *Philosophical Transactions of the Royal Society of London*, Vol. 157, 1867, pp. 49–88.
- <sup>7</sup>Boltzmann, L., "Weitere Studien über das Wärmegleichgewicht unter Gasmolekülen," *Sitz. Math.-Naturwiss. Cl. Akad. Wiss. Wien*, Vol. 66, 1872, pp. 275–370.
- <sup>8</sup>Junk, M., "Domain of Definition of Levermore's Five-Moment System," *Journal of Statistical Physics*, Vol. 93, No. 5/6, 1998, pp. 1143–1167.
- <sup>9</sup>Godunov, S. K., "Finite-Difference Method for Numerical Computations of Discontinuous Solutions of the Equations of Fluid Dynamics," *Matematicheskii Sbornik*, Vol. 47, 1959, pp. 271–306.
- <sup>10</sup>McDonald, J. G. and Groth, C. P. T., "Numerical Modeling of Micron-Scale Flows Using the Gaussian Moment Closure," Paper 2005-5035, AIAA, June 2005.
- <sup>11</sup>McDonald, J. and Groth, C. P. T., "Extended Fluid-Dynamic Model for Micron-Scale Flows Based on Gaussian Moment Closure," Paper 2008-691, AIAA, January 2008.
- <sup>12</sup>Groth, C. P. T. and McDonald, J. G., "Towards Physically-Realizable and Hyperbolic Moment Closures for Kinetic Theory," *Continuum Mechanics and Thermodynamics*, Vol. 21, 2010, pp. 467–493.
- <sup>13</sup>Hittinger, J. A., *Foundations for the Generalization of the Godunov Method to Hyperbolic Systems with Stiff Relaxation Source Terms*, Ph.D. thesis, University of Michigan, 2000.
- <sup>14</sup>Barth, T. J., "On Discontinuous Galerkin Approximations of Boltzmann Moment Systems with Levermore Closure," *Computer Methods in Applied Mechanics and Engineering*, Vol. 195, 2006, pp. 3311–3330.
- <sup>15</sup>Levermore, C. D., Morokoff, W. J., and Nadiga, B. T., "Moment Realizability and the Validity of the Navier-Stokes Approximation for Rarefied Gas Dynamics," submitted to the *Physics of Fluids*, October 1995.
- <sup>16</sup>Struchtrup, H., *Macroscopic Transport Equations for Rarefied Gas Flows*, Springer-Verlag, Berlin, 2005.
- <sup>17</sup>Struchtrup, H. and Torrilhon, M., "Regularization of Grad's 13 Moment Equations: Derivation and Linear Analysis," *Physics of Fluids*, Vol. 15, No. 9, 2003, pp. 2668–2680.



- <sup>18</sup>Struchtrup, H. and Torrilhon, M., “H Theorem, Regularization, and Boundary Conditions for the Linearized 13 Moment Equations,” *Physical Review Letters*, Vol. 99, 2007, pp. 014502.
- <sup>19</sup>Torrilhon, M. and Struchtrup, H., “Boundary Conditions for Regularized 13 Moment Equations for Micro-Channel Flows,” *Journal of Computational Physics*, Vol. 227, 2008, pp. 1982–2011.
- <sup>20</sup>McDonald, J. G., *Extended Fluid-Dynamic Modelling for Numerical Solution of Micro-Scale*, Ph.D. thesis, University of Toronto, 2010.
- <sup>21</sup>Gao, X. and Groth, C. P. T., “Parallel Adaptive Mesh Refinement Scheme for Three-Dimensional Turbulent Non-Premixed Combustion,” Paper 2008-1017, AIAA, January 2008.
- <sup>22</sup>Gao, X., *A Parallel Solution-Adaptive Method for Turbulent Non-Premixed Combusting Flows*, Ph.D. thesis, University of Toronto, August 2008.
- <sup>23</sup>Gao, X. and Groth, C. P. T., “A Parallel Solution-Adaptive Method for Three-Dimensional Turbulent Non-Premixed Combusting Flows,” *Journal of Computational Physics*, Vol. 229, No. 5, 2010, pp. 3250–3275.
- <sup>24</sup>Chapman, S. and Cowling, T. G., *The Mathematical Theory of Non-Uniform Gases*, Cambridge University Press, Cambridge, 1960.
- <sup>25</sup>Burgers, J. M., *Flow Equations for Composite Gases*, Academic Press, New York, 1969.
- <sup>26</sup>Gombosi, T. I., *Gaskinetic Theory*, Cambridge University Press, Cambridge, 1994.
- <sup>27</sup>Bhatnagar, P. L., Gross, E. P., and Krook, M., “A Model for Collision Processes in Gases. I. Small Amplitude Processes in Charged and Neutral One-Component Systems,” *Physical Review*, Vol. 94, No. 3, 1954, pp. 511–525.
- <sup>28</sup>Holway, L. H., “New Statistical Models for Kinetic Theory: Methods of Construction,” *Physics of Fluids*, Vol. 9, No. 9, 1966, pp. 1658–1673.
- <sup>29</sup>Andries, P. and Perthame, B., “The ES-BGK Model Equation with Correct Prandtl Number,” *Rarefied Gas Dynamics*, edited by T. J. Bartel and M. A. Gallis, Vol. I, American Institute of Physics, New York, 2001, pp. 30–36.
- <sup>30</sup>Andries, P., Le Tallec, P., Perlat, J.-P., and Perthame, B., “The Gaussian-BGK model of Boltzmann Equation with Small Prandtl Number,” *European Journal of Mechanics B — Fluids*, Vol. 19, 2000, pp. 813–830.
- <sup>31</sup>Hertweck, F., “Allgemeine 13-Momenten-Näherung zur Fokker-Planck-Gleichung eines Plasmas,” *Zeitschrift für Naturforschung*, Vol. 20a, 1965, pp. 1243–1255.
- <sup>32</sup>Oraevskii, V., Chodura, R., and Feneberg, W., “Hydrodynamic Equations for Plasmas in Strong Magnetic Fields — I Collisionless Approximation,” *Plasma Physics*, Vol. 10, 1968, pp. 819–828.
- <sup>33</sup>Holway, L. H., *Approximation Procedures for Kinetic Theory*, Ph.D. thesis, Harvard University, 1963.
- <sup>34</sup>Holway, L. H., “Kinetic Theory of Shock Structure Using an Ellipsoidal Distribution Function,” *Rarefied Gas Dynamics*, edited by J. H. e Leeuw, Vol. I, Academic Press, New York, 1966, pp. 193–215.
- <sup>35</sup>Holway, L. H., “The Effect of Collisional Models upon Shock Wave Structure,” *Rarefied Gas Dynamics*, edited by C. L. Brundin, Vol. I, Academic Press, New York, 1967, pp. 759–784.
- <sup>36</sup>Chodura, R. and Pohl, F., “Hydrodynamic Equations for Plasmas in Strong Magnetic Fields — II Transport Equations Including Collisions,” *Plasma Physics*, Vol. 13, 1971, pp. 645–658.
- <sup>37</sup>Demars, H. G. and Schunk, R. W., “Transport Equations for Multispecies Plasmas Based on Individual Bi-Maxwellian Distributions,” *Journal of Physics D: Applied Physics*, Vol. 12, 1979, pp. 1051–1077.
- <sup>38</sup>Brown, S. L., Roe, P. L., and Groth, C. P. T., “Numerical Solution of a 10-Moment Model for Nonequilibrium Gasdynamics,” Paper 95-1677, AIAA, June 1995.
- <sup>39</sup>Brown, S. L., *Approximate Riemann Solvers for Moment Models of Dilute Gases*, Ph.D. thesis, University of Michigan, 1996.
- <sup>40</sup>Roe, P. L., “Approximate Riemann Solvers, Parameter Vectors, and Difference Schemes,” *Journal of Computational Physics*, Vol. 43, 1981, pp. 357–372.
- <sup>41</sup>McDonald, J. G., *Numerical Modeling of Micron-Scale Flows Using the Gaussian Moment Closure*, Master’s thesis, University of Toronto, 2005.
- <sup>42</sup>McDonald, J. G., Sachdev, J. S., and Groth, C. P. T., “Gaussian Moment Closure for the Modelling of Continuum and Micron-Scale Flows with Moving Boundaries,” *Proceedings of the Fourth International Conference on Computational Fluid Dynamics, ICCFD4, Ghent, Belgium, July 10–14, 2006*, edited by H. Deconinck and E. Dick, Springer-Verlag, Heidelberg, 2009, pp. 783–788.
- <sup>43</sup>Groth, C. P. T. and McDonald, J. G., “Towards Physically-Realizable and Hyperbolic Moment Closures for Kinetic Theory,” Vol. 21, No. 6, 2009, pp. 467–493.
- <sup>44</sup>McDonald, J. G., Sachdev, J. S., and Groth, C. P. T., “Application of Gaussian Moment Closure to Micro-Scale Flows with Moving and Embedded Boundaries,” submitted to the AIAA Journal, January 2013.
- <sup>45</sup>Le Tallec, P., “A Hierarchy of Hyperbolic Models Linking Boltzmann to Navier Stokes Equations for Polyatomic Gases,” Vol. 80, 2000, pp. 779–789.
- <sup>46</sup>Bryan, G. H., “On the Present State of Our Knowledge of Thermodynamics. Part II,” Report 64–106, British Association for the Advancement of Science, 1894.
- <sup>47</sup>Harris, S., *An Introduction to the Theory of the Boltzmann Equation*, Holt, Rinehart and Winston, New York, 1971.
- <sup>48</sup>Pidduck, F., “The Kinetic Theory of a Special Type of Rigid Molecule,” *Proceedings of the Royal Society of London A*, Vol. 708, 1922, pp. 101–112.
- <sup>49</sup>Curtiss, C. F., “Kinetic Theory of Nonspherical Molecules,” *Journal of Chemical Physics*, Vol. 24, No. 2, 1956, pp. 225–241.
- <sup>50</sup>Taxman, N., “Classical Theory of Transport Phenomena in Dilute Polyatomic Gases,” *Physical Review*, Vol. 110, No. 4, 1958, pp. 1235–1239.

- <sup>51</sup>Wang Chang, C. S., Uhlenbeck, G. E., and de Boer, J., "The Heat Conductivity and Viscosity of Polyatomic Gases," *Studies in Statistical Mechanics*, edited by J. de Boer and G. E. Uhlenbeck, Vol. II, North-Holland, Amsterdam, 1964, pp. 243–268.
- <sup>52</sup>Kennard, E. H., *Kinetic Theory of Gases*, McGraw-Hill, New York, 1938.
- <sup>53</sup>Gao, X. and Groth, C. P. T., "Parallel Adaptive Mesh Refinement Scheme for Turbulent Non-Premixed Combusting Flow Prediction," Paper 2006-1448, AIAA, January 2006.
- <sup>54</sup>Gao, X. and Groth, C. P. T., "A Parallel Adaptive Mesh Refinement Algorithm for Predicting Turbulent Non-Premixed Combusting Flows," *International Journal of Computational Fluid Dynamics*, Vol. 20, No. 5, 2006, pp. 349–357.
- <sup>55</sup>Gao, X., Northrup, S. A., and Groth, C. P. T., "Parallel Solution-Adaptive Method for Two-Dimensional Non-Premixed Combusting Flows," Vol. 11, No. 2, 2011, pp. 76–95.
- <sup>56</sup>Charest, M. R. J., Groth, C. P. T., and Gülder, Ö. L., "A Parallel Solution Adaptive Method for Radiative Heat Transfer Using a Newton-Krylov Approach," *Proceedings of the 18th Annual Conference of the CFD Society of Canada, London, Ontario, Canada, May 18-19, 2010*, 2010.
- <sup>57</sup>Groth, C. P. T. and Northrup, S. A., "Parallel Implicit Adaptive Mesh Refinement Scheme for Body-Fitted Multi-Block Mesh," Paper 2005-5333, AIAA, June 2005.
- <sup>58</sup>Mathur, S. R. and Murthy, J. Y., "A Pressure-Based Method for Unstructured Meshes," Vol. 31, 1997, pp. 191–215.
- <sup>59</sup>Saad, Y. and Schultz, M. H., "GMRES: A Generalized Minimal Residual Algorithm for Solving Nonsymmetric Linear Equations," *SIAM Journal for Scientific and Statistical Computing*, Vol. 7, No. 3, 1986, pp. 856–869.
- <sup>60</sup>Saad, Y., *Iterative Methods for Sparse Linear Systems*, PWS Publishing Company, Boston, 1996.
- <sup>61</sup>Gropp, W. D., Kaushik, D. K., Keyes, D. E., and Smith, B. F., "High-Performance Parallel Implicit CFD," *Parallel Computing*, Vol. 27, 2001, pp. 337–362.
- <sup>62</sup>Northrup, S. A. and Groth, C. P. T., "Parallel Implicit Adaptive Mesh Refinement Algorithm for Solution of Laminar Combusting Flows," 14th Annual Conference of the CFD Society of Canada, Kingston, Ontario, Canada, July 16–18, 2006, July 2006.
- <sup>63</sup>Knoll, D. A., McHugh, P. R., and Keyes, D. E., "Newton-Krylov Methods for Low-Mach-Number Compressible Combustion," *AIAA Journal*, Vol. 34, No. 5, 1996, pp. 961–967.
- <sup>64</sup>Cai, X.-C., Gropp, W. D., Keyes, D. E., Melvin, R. G., and Young, D. P., "Parallel Newton-Krylov-Schwarz Algorithms for the Transonic Full Potential Equations," *SIAM Journal on Scientific Computing*, Vol. 19, No. 1, 1998, pp. 246–265.
- <sup>65</sup>Nielsen, E. J., Anderson, W. K., Walters, R. W., and Keyes, D. E., "Application of Newton-Krylov Methodology to a Three-Dimensional Unstructured Euler Code," Paper 95-1733-CP, AIAA, June 1995.
- <sup>66</sup>Sachdev, J. S. and Groth, C. P. T., "A Mesh Adjustment Scheme for Embedded Boundaries," Vol. 2, No. 6, 2007, pp. 1095–1124.
- <sup>67</sup>Sachdev, J. S., *Parallel Solution-Adaptive Method for Predicting Solid Propellant Rocket Motor Core Flows*, Ph.D. thesis, University of Toronto, April 2007.
- <sup>68</sup>Vedovotoa, J. M. and A. da Silveira Neto, A. Murab, L. F. F. d. S., "Application of the method of manufactured solutions to the verification of a pressure-based finite-volume numerical scheme," *Computers & Fluids*, Vol. 51, 2011, pp. 85–99.
- <sup>69</sup>Lam, C. K. S. and Groth, C. P. T., "Numerical Prediction of Three-Dimensional Non-Equilibrium Gaseous Flows Using the Gaussian Moment Closure," Paper 2011-3401, AIAA, June 2011.
- <sup>70</sup>Coudeville, H., Trepaud, P., and Brun, E. A., "Drag Measurements in Slip and Transition Flow," *Rarefied Gas Dynamics*, edited by J. H. de Leeuw, Vol. I, Academic Press, New York, 1965, pp. 444–466.
- <sup>71</sup>Patterson, G. N., *Introduction to the Kinetic Theory of Gas Flows*, University of Toronto Press, Toronto, 1961.
- <sup>72</sup>Torrilhon, M., "Slow gas microflow past a sphere: Analytical solution based on moment equations," *Physics of Fluids*, Vol. 22, No. 7, 2010, pp. 072001.
- <sup>73</sup>Roos, F. W. and Willmarth, W. W., "Some Experimental Results on Sphere and Disk Drag," *AIAA Journal*, Vol. 9, 1971, pp. 285–291.
- <sup>74</sup>Liebster, M., "Über den Widerstand von Kugeln," *Annalen der Physik*, Vol. 83, 1927, pp. 541–562.
- <sup>75</sup>Flemmer, R. L. C. and Banks, C. L., "On the drag coefficient of a sphere," *Powder Technology*, Vol. 48, 1986, pp. 217–221.